

Glutamate Dynamics Determine the Magnitude of Hebbian Synaptic Plasticity

By:

Jocelyn Ruth Barnes

A thesis submitted to the school of graduate studies in partial fulfilment of the requirements for the degree of Master of Science in Medicine (Neuroscience)

Faculty of Medicine

Memorial University of Newfoundland

May 2019

St John's

Newfoundland

Abstract

Increasing evidence suggests that synaptic NMDA receptors (NMDARs) promote long term potentiation (LTP) while extrasynaptic NMDARs inhibit LTP and promote long term depression (LTD). Glutamate transporters maintain this balance by rapidly clearing glutamate from the extracellular space. In many disease states, transporter dysfunction is thought to underlie LTP deficits. However, the precise relationship between extracellular glutamate dynamics and LTP is unknown. Here, we used an optogenetic sensor of glutamate to monitor glutamate dynamics in real-time during LTP induction.

Pharmacologically blocking glutamate transporters slowed clearance and inhibited LTP magnitude in a concentration-dependent manner. Surprisingly, impaired glutamate clearance caused rapid NMDAR desensitization and simultaneous three-fold increases in postsynaptic calcium through L-type voltage gated calcium channels. Overall, our data characterize the relationship between glutamate dynamics and LTP, and identify a novel mechanism underlying LTP impairment due to slow glutamate clearance. These results may be applicable to neurodegenerative diseases associated with impaired synaptic plasticity and glutamate transporter dysfunction.

Acknowledgements

I would like to thank my supervisor, Dr. Matthew Parsons, for all his guidance, support and encouragement. Without him, none of the work presented within this thesis would be possible. His combination of hands on guidance and trust in my own abilities has really allowed me to grow as a researcher.

I would also like to thank my supervisory committee, Drs. Craig Moore and Qi Yuan, for their expert opinions and support during my Masters.

Lastly, I would like to thank my lab members, other faculty members, graduate students and support staff for all their help and for challenging me to become a better researcher. I would like to especially thank our research assistant, Firoozeh Nafar. Her guidance, words of encouragement, and help with anything and everything really made my time in the lab an absolute joy. Research is much easier when you have a community supporting and encouraging you; therefore, I appreciate each person with whom I have interacted during my Masters.

Table of Contents

Abstract	ii
Acknowledgements	iii
List of Figures	vii
List of Abbreviations	ix
Co-Authorship Statement.....	xiii
Chapter 1 – Introduction	1
1.1 Synaptic Transmission	2
1.1.1 Long Term Potentiation	2
1.1.2 Long Term Depression	5
1.1.3 Intracellular Regulation of LTP and LTD	6
1.2 Initiating NMDAR-dependent LTP and LTD	7
1.2.1 Subunit Hypothesis	7
1.2.2 Localization Hypothesis	9
1.2.3 Unified Hypothesis	10
1.3 Regulation of Extracellular Glutamate	11
1.3.1 Glutamate Transporters	12
1.3.2 Role of Glutamate Transporters in the Brain.....	16
1.3.3 Measuring Glutamate Clearance.....	17

1.4 Glutamate Dysregulation in Disease States	19
1.4.1 Alzheimer Disease	19
1.5 Hypothesis	21
1.6 Aims of this thesis project	21
Chapter 2 – Methodology	22
2.1 Animals	22
2.2 Stereotaxic Surgery	22
2.3 Slice Preparation	24
2.4 Real-time Imaging of Glutamate or Calcium Biosensors	24
2.5 Imaging Analysis.....	25
2.6 Electrophysiology.....	26
2.7 Immunofluorescence	27
2.8 Immunofluorescence Imaging and Analysis	28
2.9 Drugs	29
2.10 Statistical Analysis	29
Chapter 3 – Results	31
3.1 Visualizing real-time extracellular glutamate dynamics in the hippocampus.....	31
3.2 Non-selective glutamate transporter blockade increases extracellular glutamate accumulation and impairs TBS-LTP.....	35

3.3 Selective blockade of GLT-1 slows glutamate clearance but does not impair LTP	49
3.4 Variations in glutamate dynamics does not correlate with LTP magnitude in control conditions	55
3.5 Glutamate transporter inhibition does not impair LTP through excessive activation of NMDARs or recruitment of common LTD pathways	61
3.6 Glutamate transporter inhibition impairs LTP by activation of L-type voltage gated calcium channels and calpain	72
Chapter 4 – Discussion	79
4.1 Three-fold deficits in glutamate clearance are required to impair synaptic plasticity	80
4.2 Mechanism of TBOA-mediated LTP impairment	81
4.3 Relevance to Neurodegenerative Disease	86
4.4 Conclusion.....	87
References	88

List of Figures

Figure 1: Schematic of a typical tripartite synapse.	14
Figure 2: iGluSnFR expression and responses in hippocampus.	33
Figure 3: Blocking all glutamate transporters slows glutamate clearance in a dose dependant manner.	36
Figure 4: Repeated TBS does not alter glutamate clearance rates during subsequent theta bursts.	39
Figure 5: Blocking glutamate transporters impairs glutamate clearance and LTP.	43
Figure 6: Blocking glutamate transporters impairs glutamate clearance and impairs LTP in FVB mice.	47
Figure 7: Blocking GLT-1 slows glutamate clearance in a dose dependant manner.	50
Figure 8: Blocking GLT-1 slows glutamate clearance during a theta burst protocol without affecting the magnitude of LTP.	53
Figure 9: The presence of iGluSnFR in the hippocampus does not significantly alter the magnitude of potentiation post LTP induction.	56
Figure 10: Natural variation in glutamate clearance is not associated with variability in percent potentiation.	59
Figure 11: TBOA induced LTP impairment is not mediated by NMDAR overactivation or recruitment of common LTD pathways.	64
Figure 12: pERK is increased post-LTP induction in the presence of 15 μ M TBOA.	67
Figure 13: Impaired glutamate clearance causes desensitization of NMDARs during theta burst stimulation.	70

Figure 14: The presence of 15 μ M TBOA during theta burst stimulation increases post-synaptic calcium which requires activation of NMDARs.73

Figure 15: The presence of 15 μ M TBOA during TBS increases post-synaptic calcium via influx through VGCC to impair LTP.....77

List of Abbreviations

°C: Degrees Celsius

%: Percent

% Δ F/F: Percent change in fluorescence over fluorescence

μ A: Microamperes

μ L: Microlitre

μ m: Micrometer

μ M: Micromolar

AAV: Adenosine associated virus

ACSF: Artificial cerebrospinal fluid

AD: Alzheimer Disease

AIDA: (*RS*)-1-Aminoindan-1,5-dicarboxylic acid

AMPA: α -amino-3-hydroxyl-5-methyl-4-isoxazole-propionate

AMPA: α -amino-3-hydroxyl-5-methyl-4-isoxazole-propionate receptor

AU: Arbitrary units

CaMKII: Ca²⁺/calmodulin-dependent protein kinase II

CaMKIV: Ca²⁺/calmodulin-dependent protein kinase IV

CREB: cAMP response element-binding protein

D-APV: D-(-)-2-Amino-5-phosphonopentanoic acid

Dan: Dantrolene

DAPI: 4',6-diamidino-2-phenylindole

DHK: Dihydrokainic acid

EAAC1: excitatory amino acid carrier 1

EAAT1: Excitatory amino acid transporter 1

EAAT2: Excitatory amino acid transporter 2

EAAT3: Excitatory amino acid transporter 3

EAAT4: Excitatory amino acid transporter 4

EAAT5: Excitatory amino acid transporter 5

EPSC: Excitatory postsynaptic current

ERK: Extracellular regulated kinase

fEPSP: field excitatory postsynaptic potential

F/F: Fluorescence/ fluorescence

GCaMP6f: Green fluorescent–calmodulin–M13 fusion protein 6 fast

GFP: Green fluorescent protein

GLT-1: Glutamate transporter-1

GLAST: Glutamate aspartate transporter

GSK3: Glycogen synthetase kinase 3

HFS: High frequency stimulation

Hz: Hertz

iGluSnFR: Intensity-based glutamate sensing fluorescent reporter

IOS: Intrinsic optical signal

kg: kilogram

kHz: Kilohertz

L-VGCC: L-type voltage gated calcium channel

LED: Light-emitting diode

LFS: Low frequency stimulation

LTD: Long term depression

LTP: Long term potentiation

M: Molar

MΩ: Megaohms

MAPK: Microtubule associated protein kinase

MDL 28170: *N*-[*N*-[(Phenylmethoxy)carbonyl]-*L*-valyl]-phenylalaninal

mg: Milligram

mGluR: Metabotropic glutamate receptor

min: Minute

MK-801: (5*S*,10*R*)-(+)-5-Methyl-10,11-dihydro-5*H*-dibenzo[*a,d*]cyclohepten-5,10-imine

Maleate

mL: Millilitre

mM: Millimolar

mm: Millimetre

ms: Millisecond

NASPM: 1-Naphthylacetyl spermine trihydrochloride

Nif: Nifedipine

nL: Nanolitre

NMDA: *N*-methyl-D-aspartate

NMDAR: *N*-methyl-D-aspartate receptor

PBS: Phosphate buffered saline

pERK: Phosphorylated extracellular regulated kinase

PKA: Protein kinase A

PP1: Protein phosphatase 1

PSD: Postsynaptic density

ROI: region of interest

RM ANOVA: Repeated measure ANOVA

RT: Room temperature

s: Second

SB 415286: 3-[(3-Chloro-4-hydroxyphenyl)amino]-4-(2-nitrophenyl)-1H-pyrrol-2,5-dione

SCOP: Suprachiasmatic nucleus circadian oscillatory protein

STC: Synaptically-activated transporter current

SEM: Standard Error of Mean

TBOA: DL-threo- β -Benzyloxyaspartic acid

TBS: Theta burst stimulation

VSD: Voltage sensitive dye

Co-Authorship Statement

All experiments within this thesis were conducted by myself, Jocelyn Ruth Barnes, with the exception of Figure 12 and Figure 15b-g. These experiments were done with the help of Dr. Bandhan Mukherjee, Dr. Matthew P. Parsons and Mrs. Firoozeh Nafar.

Chapter 1 – Introduction

Synaptic plasticity, the activity-dependent strengthening or weakening of synaptic connections, represents the neurological underpinnings of cognitive function. Persistent synaptic plasticity can be separated into two broad phenomena: long-term potentiation (LTP) and long-term depression (LTD), which represent a synapse's ability to strengthen or weaken, respectively, in response to different stimulus inputs. This modification in connectivity can be mediated by both pre- and/or post-synaptic mechanisms depending on the pathway under investigation (Malenka and Bear, 2004). To add to the complexity, many synapses can undergo multiple forms of both LTP and LTD, making the interactions between neural populations quite versatile.

LTP was first discovered in the early 1970s when Bliss and Lomo electrically stimulated the perforant pathway projecting from the entorhinal cortex to the dentate gyrus, a subregion within the hippocampus. Using continuous trains of stimulation, they found that responses in the dentate gyrus increased in magnitude for up to 10 hours (Bliss and Lomo, 1973). This ground-breaking research spawned the field of synaptic plasticity that we know today. In addition, these pioneering studies eventually led to the discovery of many types of synaptic plasticity at numerous excitatory and inhibitory synapses throughout the brain (Malenka and Bear, 2004; Kauer and Malenka, 2007; Bains et al., 2015; Bliss et al., 2016). Today, one of the most commonly studied forms of LTP is N-methyl D-aspartate (NMDA) receptor (NMDAR) dependent LTP at the Schaffer collateral-CA1 pathway within the hippocampus, a subregion that has since been established as have a role in learning and memory (Bliss and Collingridge, 1993).

1.1 Synaptic Transmission

When the Schaffer collateral pathway is stimulated, an action potential results in the release of glutamate, the most abundant excitatory neurotransmitter, into the extracellular space. This area of release is known as the synaptic cleft where pre- and post-synaptic neurons are in very close proximity. Glutamate is then free to diffuse across the synaptic cleft and bind to postsynaptic glutamate receptors (Bliss and Collingridge, 1993; Malenka and Bear, 2004; Kauer and Malenka, 2007). Of specific interest to the present thesis are two ionotropic glutamate receptors: NMDARs, as previously mentioned, and α -amino-3-hydroxy-5-methyl-4-isoxazolepropionic acid (AMPA) receptors (AMPA). At typical neuronal resting membrane potentials, NMDARs contain a magnesium ion block within the receptor pore which prevents ion influx (Nowak et al., 1984). Therefore, basal glutamatergic synaptic transmission is largely mediated by AMPARs. When glutamate binds to AMPARs, a conformational change causes the ion channel to open allowing the influx of positively-charged ions, predominately sodium, into the postsynaptic cell. This influx of positive current is known as an excitatory postsynaptic current (EPSC), and results in the depolarization of the postsynaptic neuron. EPSCs can summate in both time and space to determine whether the postsynaptic neuron fires an action potential (Piskorowski and Chevaleyre, 2012).

1.1.1 Long Term Potentiation

During LTP, the size of the EPSC increases, enhancing the probability that the postsynaptic neuron will fire an action potential. LTP can be separated into three distinct

phases: induction, expression and maintenance (Malenka and Bear, 2004). As mentioned, NMDAR-dependent LTP at the Schaffer collateral-CA1 synapse is the most commonly studied form of LTP and is the focus of the present thesis; therefore, all mechanisms discussed here refer to this type of LTP at this synapse. During the high activity patterns typically required for LTP induction (Zhu et al., 2015), sustained presynaptic activity results in depolarization of the postsynaptic neuron (Bliss and Collingridge, 1993; Malenka and Bear, 2004; Kauer and Malenka, 2007). This depolarization removes the magnesium block from NMDARs. Subsequent glutamate binding to NMDARs results in the influx of sodium as well as calcium into the postsynaptic neuron. Calcium influx initiates intracellular signalling cascades that ultimately strengthens the synaptic connection (Bliss and Collingridge, 1993; Malenka and Bear, 2004; Kauer and Malenka, 2007). Depending on the LTP induction protocol, calcium can activate different intracellular signalling pathways (Baudry et al., 2015; Zhu et al., 2015). Two of the most common LTP induction protocols are high frequency stimulation (HFS; 100 pulses at 100 Hz) (Li et al., 2011) and theta burst stimulation (TBS; 10 bursts at 5 Hz with each burst consisting of 4 pulses at 100 Hz) (Volianskis et al., 2013). Both HFS and TBS results in calcium influx through NMDARs that activates calcium/calmodulin dependent protein kinase II (CaMKII) (Lisman, 1994; Malenka and Bear, 2004; Huganir and Nicoll, 2013).

Interestingly, after this initial CaMKII activation, different intracellular signalling cascades are recruited with these two induction protocols (Baudry et al., 2015; Zhu et al., 2015). HFS results in the activation of protein kinase A, which can phosphorylate several proteins involved in LTP including the GluA1 subunit of AMPARs (Huganir and Nicoll, 2013; Zhu et al., 2015; Hell, 2016). In contrast, TBS results in calcium influx through

NMDARs that activates calpain-1 (Baudry et al., 2015; Zhu et al., 2015; Baudry and Bi, 2016). Calpains, including calpain-1 and calpain-2, are proteolytic calcium-dependent enzymes which have recently received great interest in the plasticity field for their opposing effects on synaptic plasticity (Wang et al., 2014; Baudry and Bi, 2016; Liu et al., 2016b). Calpain-1 activation leads to the breakdown of Suprachiasmatic nucleus circadian oscillatory protein (SCOP), a negative regulator of extracellular regulated kinase (ERK) (Baudry et al., 2015; Zhu et al., 2015; Baudry and Bi, 2016). Increased ERK activation causes an increase in AMPAR trafficking to the synapse (Giovannini, 2006; Baudry et al., 2015). Thus, calpain-1 activity facilitates LTP via ERK disinhibition.

The result, or expression of LTP, after activation of these two intracellular pathways remains the same: increased synaptic transmission via AMPARs. This can be achieved through phosphorylation of existing AMPARs to increase their conductance, lateral diffusion and stabilization within the post synaptic density (PSD) of existing surface AMPARs, or exocytosis of new AMPARs (Malenka and Bear, 2004; Giovannini, 2006; Kessels and Malinow, 2009; Opazo et al., 2012; Huganir and Nicoll, 2013; Baudry et al., 2015; Zhu et al., 2015; Hell, 2016). The increase in number or conductance of AMPARs allows more sodium to enter the postsynaptic neuron in response to the same presynaptic trigger, increasing the probability that the postsynaptic neuron will reach threshold of depolarization and fire an action potential.

The last phase of LTP is maintenance, which requires gene transcription and protein synthesis in order to for LTP to be sustained over multiple hours (Bliss and Collingridge, 1993; Malenka and Bear, 2004). Microtubule associated protein kinase

(MAPK), protein kinase A (PKA) and CaMKIV all translocate the electrochemical signal from the synapse to the cell body where they can activate cAMP response element-binding protein (CREB) and immediate early genes, such as c-Fos and Homer, to initiate long-term changes at the synapse (Xing et al., 1996; Malenka and Bear, 2004; Sweatt, 2004; Hardingham and Bading, 2010; Nakahata and Yasuda, 2018). These long-term changes, such as a larger dendritic spine (Bosch et al., 2014) and an increase in filamentous actin (Bosch et al., 2014; Zhu et al., 2015), accommodate the increase in postsynaptic receptors associated with LTP.

1.1.2 Long Term Depression

Paradoxically, at these same synapses, NMDAR-dependent LTD can also be initiated (Malenka and Bear, 2004; Peineau et al., 2007). NMDAR-dependent LTD is typically induced by low frequency stimulation (LFS) (Li et al., 2009) and results in a reduction in EPSC size. It has been well established that NMDAR activation is required for this form of LTD; however, there is still debate over whether this form of LTD requires ion influx through NMDARs or whether it results from a metabotropic function of NMDARs (Kessels et al., 2013; Nabavi et al., 2013b, 2013a; Volianskis et al., 2015; Dore et al., 2016). Many labs have found that blocking the actions of NMDAR co-agonists glycine or serine, or using an intracellular calcium chelator can prevent LTD (Cummings et al., 1996; Volianskis et al., 2015) while others have found that glutamate binding without ion influx is sufficient for LTD (Nabavi et al., 2013b; Dore et al., 2016). Glutamate binding without ion influx was analyzed by incubating acute slices in a

saturating concentration of MK-801, an NMDAR antagonist binding within the receptor pore, for 3 hours prior to recording and LTD induction. These differences appear to be due to subtle discrepancies in methodologies and may suggest that LTD can occur both without ion influx and with small amounts of calcium entry.

Nevertheless, NMDAR-dependent LTD activates calcineurin which inhibits inhibitor-1 and in turn, activates protein phosphatase 1 (PP1) (Mulkey et al., 1994; Malenka and Bear, 2004; Peineau et al., 2008). PP1 activity results in dephosphorylation and clathrin-mediated endocytosis of AMPARs (Malenka and Bear, 2004; Peineau et al., 2008). This PP1-mediated decrease in postsynaptic AMPAR content is also due to regulation of glycogen synthetase kinase (GSK3) by PP1. PP1 dephosphorylates and therefore, activates GSK3 post-LTD induction (Morfini et al., 2004; Lee et al., 2005; Szatmari et al., 2005; Peineau et al., 2007, 2008). Inhibition of GSK3 prevents the expression of LTD (Peineau et al., 2007, 2008). GSK3 associates with AMPARs in the synapse to cause their endocytosis (Peineau et al., 2008).

1.1.3 Intracellular Regulation of LTP and LTD

GSK3 has become very popular in synaptic plasticity research for its ability to guide plasticity towards potentiation or depression. GSK3 is expressed throughout the brain and has widespread functions. As mentioned previously, upon activation of the LTD pathway, GSK3 is dephosphorylated, and therefore, activated (Peineau et al., 2008). Inhibition of GSK3 prevents the expression of LTD while LTP remains unaffected (Peineau et al., 2007, 2008). In addition, GSK3 activity is prevented 10 minutes after LTP

induction and lasting up to an hour (Peineau et al., 2007, 2008). These results indicate a crucial role of GSK3 in the regulation of synapse strengthening or weakening. While this explains how these pathways can be regulated intracellularly, this does not explain how a single group of NMDARs can initiate either the LTP or LTD pathway.

1.2 Initiating NMDAR-dependent LTP and LTD

Since LTP and LTD can be initiated at the same synapse by the same type of ionotropic glutamate receptor, these processes must be tightly regulated to allow memory formation and normal cognition. As mentioned previously, different stimulation parameters have opposing results on synapse strength with HFS and TBS inducing NMDAR-dependent LTP and LFS inducing NMDAR-dependent LTD (Malenka and Bear, 2004). Several hypotheses have emerged to describe the regulation of LTP and LTD including the subunit hypothesis, localization hypothesis and a unified hypothesis which combines both the subunit and localization hypotheses.

1.2.1 Subunit Hypothesis

NMDARs are tetrameric receptors with two obligatory GluN1 subunits. The other two subunits can be any combination of GluN2A-D or GluN3A-B (Paoletti et al., 2013). In the hippocampus, the majority of NMDARs contain either GluN2A and/or GluN2B; therefore, hippocampal NMDARs are typically diheteromeric with two GluN1 subunits and either two GluN2A subunits or two GluN2B subunits, or triheteromeric with two

GluN1 subunits, one GluN2A subunit and one GluN2B subunit. Glutamate binds directly to the GluN2A or GluN2B subunits, and each type of NMDAR exhibits different kinetics and open probabilities upon glutamate binding; GluN2A-containing NMDARs have a higher open probability and faster decay than GluN2B-containing NMDARs (Paoletti et al., 2013). This led researchers to postulate that GluN2A-containing and GluN2B-containing NMDAR trigger different intracellular signalling cascades and therefore, activate either LTP-promoting or LTD-promoting pathways, respectively. During induction of LTP, the charge transfer through GluN2A-containing NMDARs outweighs the charge transfer through GluN2B-containing NMDARs (Erreger et al., 2005; Paoletti et al., 2013). In addition, knockout of the GluN2A subunit or NMDAR blockade using the GluN2A-preferring antagonist, NVP-AAM077 both prevent LTP (Sakimura et al., 1995; Liu et al., 2004; Paoletti et al., 2013). Supporting this dichotomous role of NMDARs, knockout of the GluN2B subunit or blockade using GluN2B-specific antagonists ifenprodil or Ro 25-6981, prevents hippocampal LTD (Liu et al., 2004; Brigman et al., 2010; Paoletti et al., 2013). To summarize, the subunit hypothesis states that GluN2A-containing NMDARs preferentially initiate LTP while GluN2B-containing NMDARs initiate LTD. While this is an attractive hypothesis, it is important to note that there are no highly selective blockers for GluN2A-containing NMDARs, and that these studies largely ignore triheteromeric NMDARs, which may account for 30% of NMDARs in the hippocampus (Al-Hallaq et al., 2007; Kellermayer et al., 2018). The role of triheteromeric NMDARs in LTP and/or LTD is still unknown.

1.2.2 Localization Hypothesis

Another attractive and well-cited hypothesis describing the initiation of LTP or LTD pathways is the localization hypothesis. This hypothesis states that synaptic NMDARs promote LTP and extrasynaptic NMDARs promote LTD (Lu et al., 2001; Pickard et al., 2001; Liu et al., 2004; Papouin et al., 2012). For NMDARs to be activated, simultaneous binding of glutamate and glycine or serine is required. When glycine is applied to culture during spontaneous glutamate release, a sustained increase in EPSC amplitude is observed (i.e., LTP) (Lu et al., 2001). During spontaneously-occurring glutamate release (i.e., in the absence of external stimulation), it is generally assumed that only synaptic NMDARs will be activated. Pre-treatment with 1-5 μ M MK-801, an NMDAR antagonist that irreversibly blocks the pore of open NMDARs, prevented the increase in EPSC amplitude after glycine application. Since NMDARs need to open for MK-801 to enter the channel pore, it is assumed that only synaptic NMDARs would be blocked under such conditions. Using MK-801 in the same manner to block synaptic NMDARs, NMDA bath application or electrical stimulation can still induce LTD (Lu et al., 2001; Liu et al., 2004). The conclusion drawn from the latter experiments is that the selective activation of extrasynaptic NMDARs is sufficient to trigger LTD.

Synaptic and extrasynaptic NMDARs have also been shown to require different co-agonists (Papouin et al., 2012). By degrading serine, they found that synaptic NMDAR-dependent EPSCs require serine as a co-agonist. When glycine is degraded, synaptic NMDAR-dependent EPSCs are unaffected. However, glycine degradation prevents tonic activation of NMDARs which has previously been shown to involve

extrasynaptic NMDARs (Le Meur et al., 2007). Despite using indirect methods to study synaptic versus extrasynaptic NMDARs, these studies suggest that synaptic NMDARs promote synapse strengthening while extrasynaptic NMDARs promote synapse weakening.

1.2.3 Unified Hypothesis

The final hypothesis of interest to the present thesis is the unified hypothesis, which combines both the subunit and localization hypotheses. This postulates that synaptic, GluN2A-containing NMDARs initiate LTP and extrasynaptic, GluN2B-containing NMDARs initiate LTD (Steigerwald et al., 2000; Groc et al., 2006; Hardingham and Bading, 2010; Paoletti et al., 2013). Steigerwald and colleagues found that truncation of the C-terminal domain of the GluN2A subunit did not alter function of NMDARs but did significantly reduce the amount of synaptic NMDARs as detected by immunofluorescence (Steigerwald et al., 2000). Using single particle tracking, Groc and colleagues have found that GluN2A subunits are more stable within the synapse than GluN2B subunits (Groc et al., 2006), suggesting that the more stable GluN2A subunits are expressed at higher levels within the synapse than GluN2B subunits, which are freer to move into and out of the synaptic space. This increased mobility results in GluN2B-containing NMDARs to be more commonly found at peri- and extrasynaptic subcellular localizations. However, there have been other studies suggesting that there is no difference in subunit expression based on subcellular location (Harris and Pettit, 2007; Petralia et al., 2010). At 3 weeks of age, the rat hippocampus showed no differences in

GluN2B-containing NMDARs based on synaptic or extrasynaptic compartments (Harris and Pettit, 2007). The discrepancies seen here are likely due to differences in the age or species used, and therefore, the unified hypothesis remains attractive and well-cited within the literature, especially in many neurodegenerative diseases where a dysfunction in synaptic plasticity is observed (discussed below).

1.3 Regulation of Extracellular Glutamate

Since synaptic NMDARs are thought to initiate LTP and extrasynaptic NMDARs are thought to initiate LTD, extracellular glutamate dynamics must be tightly regulated to facilitate potentiation. Glutamate cannot be metabolized in the extracellular space and therefore, diffusion and transporter-mediated glutamate uptake shape the spatiotemporal dynamics of synaptically-released glutamate (Rothstein et al., 1994; Danbolt, 2001). Glutamate transporters maintain the extracellular glutamate concentration at sub-micromolar levels by relying on the electrochemical gradient of sodium (Drejer et al., 1982; Levy et al., 1993; Danbolt, 2001; Tzingounis and Wadiche, 2007). Three sodium ions and one hydrogen ion are co-transported with each glutamate molecule while one potassium ion is counter-transported which allows transporters to rapidly remove glutamate from the extracellular space, even when the glutamate concentration within the cell becomes higher than in the extracellular space.

1.3.1 Glutamate Transporters

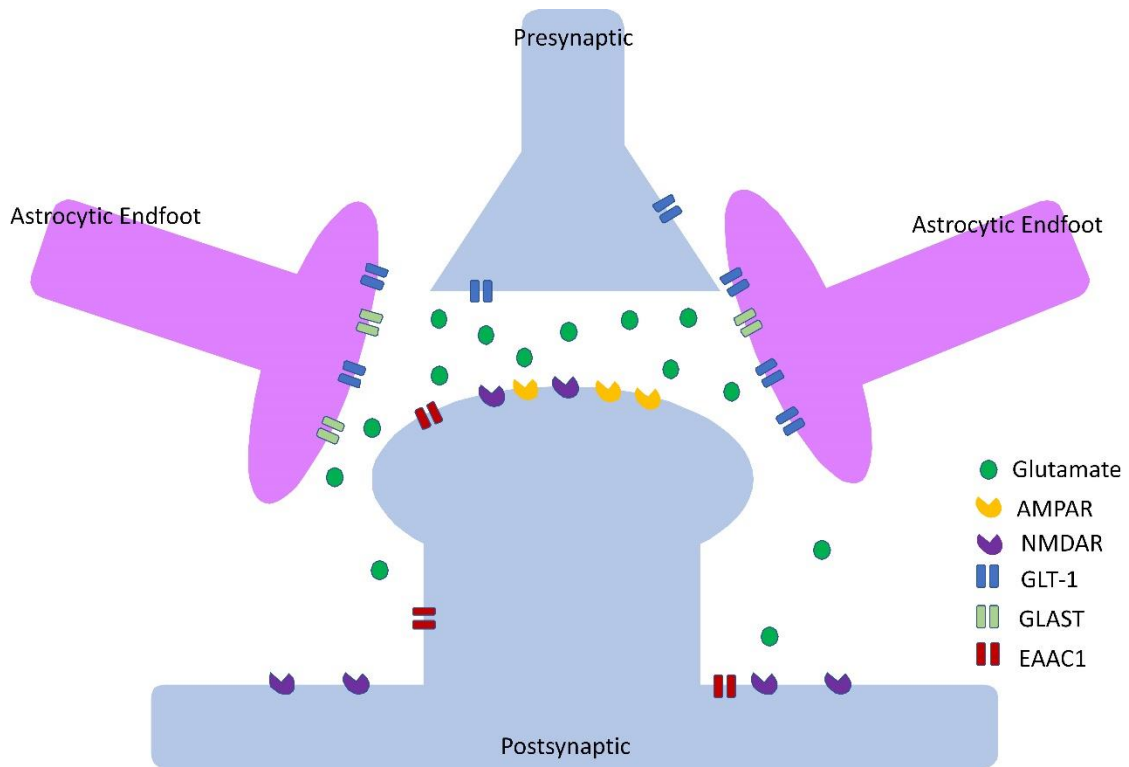
There are five subtypes of glutamate transporters known as excitatory amino acid transporters 1-5 (EAAT1-5). The expression of these transporter subtypes varies by brain region and cell type. The predominant transporters within the hippocampus are EAAT1-3; EAAT4 and EAAT5 are largely expressed in the cerebellum and retina, respectively (Danbolt, 2001; Tzingounis and Wadiche, 2007). EAAT1, EAAT2, and EAAT3 are also known as GLAST, GLT-1, and EAAC1, respectively and will be referred to as such for the remainder of this thesis. GLT-1 is found primarily on astrocytes, with a small proportion expressed neuronally (Fig 1) (Kanai and Hediger, 1992; Levy et al., 1993; Aoyama et al., 2006; Tzingounis and Wadiche, 2007; Holmseth et al., 2012; Vandenberg and Ryan, 2013). GLAST and EAAC1 are expressed exclusively on astrocytes and neurons, respectively.

Astrocytic endfeet surround hippocampal synapses in a configuration known as a tripartite synapse (Perea et al., 2009), and these endfeet contain high levels of both GLAST and GLT-1 (Kanai and Hediger, 1992; Levy et al., 1993; Aoyama et al., 2006; Tzingounis and Wadiche, 2007; Holmseth et al., 2012; Vandenberg and Ryan, 2013). Glutamate transporters form complexes of homodimers, homotrimers, and homotetramers within astrocytic endfeet (Haugeto et al., 1996). GLAST and GLT-1 do not form complexes with each other but localize in close proximity within the astrocytic membrane. Complexes of GLAST or GLT-1 allow a large number of transporters to be present within a relatively small area of the astrocytic membrane. Neuronal GLT-1 is primarily expressed on the presynaptic membrane while EAAC1 is primarily expressed

on the soma and dendrites (Fig 1) (Holmseth et al., 2012). A high density of glutamate transporters in the tripartite synapse allows glutamate to be cleared quickly and efficiently following release, thereby preventing glutamate spillover from the synapse and limiting activation of extrasynaptic NMDARs.

Figure 1: Schematic of a typical tripartite synapse.

Astrocytic endfeet surround the synapse and help prevent glutamate spillover into the extrasynaptic region and neighbouring synapses. GLT-1, the most abundant glutamate transporter, is located predominantly on astrocytes with some expression found on presynaptic neurons. GLAST is exclusively astrocytic and EAAC1 is located predominantly on the dendrites and soma of neurons.



1.3.2 Role of Glutamate Transporters in the Brain

GLT-1 is the most abundant glutamate transporter and is thought to be responsible for the majority of uptake within the hippocampus (Otis and Kavanaugh, 2000; Danbolt, 2001; Holmseth et al., 2012; Vandenberg and Ryan, 2013). Knockout of GLAST and GLT-1 has shown that these transporters are vital for brain development and survival (Tanaka et al., 1997; Otis and Kavanaugh, 2000; Matsugami et al., 2006). Similarly, knockout of GLT-1 alone causes increased susceptibility to cortical injury and seizures due to increased basal levels of glutamate (Tanaka et al., 1997; Petr et al., 2015). Knockout of GLAST alone does cause an increase in the number of postsynaptic glutamate receptors within the hippocampus but the majority of studies focus on the reduction in cerebellar functioning as this is where GLAST is most prevalent (Watase et al., 1998; Ueda et al., 2002).

The neuronal transporter, EAAC1 is expressed at approximately a hundredth of the GLT-1 concentration (Holmseth et al., 2012). Acting as a buffer of extracellular glutamate, EAAC1 can bind glutamate and release it back into the extracellular space, slowing glutamate clearance and limiting NMDAR activity (Scimemi et al., 2009). It has been suggested EAAC1 is less important than GLT-1 and GLAST for glutamate clearance (Peghini et al., 1997; Aoyama et al., 2006; Vandenberg and Ryan, 2013). In mice lacking EAAC1, there are no detectable differences in development, function of neurons, or changes in hippocampal dependent memory as assessed by the Morris water maze (Peghini et al., 1997). Age-dependent brain atrophy has been observed in EAAC1 knockout mice; however this is thought to be due to the transporter's ability to transport

cysteine, which is important in metabolic signalling (Aoyama et al., 2006; Vandenberg and Ryan, 2013).

1.3.3 Measuring Glutamate Clearance

The most commonly used preparation to study glutamate clearance is the synaptosome preparation (Dodd et al., 1981; Raiteri and Raiteri, 2000; Li et al., 2009; Petr et al., 2015; Danbolt et al., 2016). Synaptosomes are pinched off nerve endings onto which exogenous radiolabeled glutamate can be applied. How quickly this exogenous glutamate is taken up into the synaptosomes is quantified by liquid scintillation. However, synaptosomes are often not pure neuronal preparations, and depending on the lab, may contain small or large amounts of astrocytic tissue. Surprisingly, it has been known for decades that astrocytes make a larger contribution to the glutamate clearance rate compared to neurons (Currie and Kelly, 1981); yet synaptosomes still represent the most commonly used preparation to study glutamate clearance. Recently, it has been shown that synaptosomes overemphasize the neuronal contribution to glutamate clearance (Petr et al., 2015). In addition, synaptosomes lack physiological relevance in that they do not recapitulate typical tripartite synaptic structure (Perea et al., 2009), and are unable to mimic physiological glutamate release.

Synaptically activated transporter currents (STCs), another common technique used to measure glutamate clearance, are currents recorded through astrocytes (Bergles and Jahr, 1997; Scimemi et al., 2009, 2013). In this preparation, an individual astrocyte is targeted for patch-clamp recording, electrical stimulation is used to evoke glutamate

release from nerve terminals in brain slices, and due to the co-transport of sodium and glutamate, a positive current into the astrocyte can be measured. From this current influx, the rate of glutamate uptake into astrocytes is calculated. While this approach is more physiologically relevant than the synaptosome preparation as it can be used *in situ*, STCs are technically demanding and time consuming, they only sample glutamate dynamics at a single astrocyte and they are reduced to undetectable levels when transporters are dysfunctional. In addition, it is believed that glutamate clearance from the synaptic cleft is much faster than that experienced on the astrocytic surface (Bergles and Jahr, 1997; Bergles et al., 1997; Diamond and Jahr, 1997). Therefore, glutamate clearance may differ in distinct microdomains. In all, more relevant techniques are required to monitor glutamate clearance at the neuronal surface in real-time.

A novel optogenetic tool, the intensity-based glutamate sensing fluorescent reporter (iGluSnFR), has recently been developed which can monitor glutamate dynamics in real-time and *in situ* (Marvin et al., 2013). Once expressed in any brain region, this virally-encoded glutamate sensor contains an extracellular binding domain which is highly selective for glutamate. Upon glutamate binding, a conformational change in the circular green fluorescent protein (GFP) causes an increase in fluorescent intensity. When glutamate unbinds from iGluSnFR, fluorescence intensity returns to the low basal levels initially present. The change in fluorescent intensity is then quantified to measure extracellular glutamate release and clearance.

1.4 Glutamate Dysregulation in Disease States

Several studies have shown that dysfunction of GLT-1 alters the time-course of synaptically released glutamate and NMDAR signalling (Bergles et al., 1997; Diamond and Jahr, 1997; Katagiri et al., 2001; Tzingounis and Wadiche, 2007; Koeglsperger et al., 2013). Dysfunction of glutamate transporters has been observed in a number of central nervous system disorders including traumatic brain injury, epilepsy, amyotrophic lateral sclerosis, schizophrenia, Huntington disease, and Alzheimer disease (AD) (Liévens et al., 2001; Yi and Hazell, 2006; Miller et al., 2008; Li et al., 2009, 2011; Faideau et al., 2010; Mookherjee et al., 2011; Scimemi et al., 2013; Petr et al., 2013, 2015; Soni et al., 2014; Tu et al., 2014; Parsons et al., 2014; Varga et al., 2015; Lei et al., 2016). Of these, AD is associated with severe memory dysfunction and plasticity deficits within the hippocampus (Townsend et al., 2006a; Welsby et al., 2007; Li et al., 2009, 2011; Varga et al., 2015; Lei et al., 2016). Therefore, the remainder of this section will focus on AD.

1.4.1 Alzheimer Disease

AD, characterized by debilitating cognitive decline, is the most common neurodegenerative disease. Amyloid beta ($A\beta$) is a toxic protein fragment that builds up in the AD brain (Selkoe and Hardy, 2016), and is well known to impair LTP induction (Townsend et al., 2006b; Welsby et al., 2007; Li et al., 2009, 2011; Varga et al., 2015; Lei et al., 2016), providing a cellular mechanism to help explain the cognitive decline in AD. It is widely accepted that $A\beta$ impairs glutamate clearance, thereby prolonging the time-course of extracellular glutamate which results in an LTP impairment (Li et al., 2009,

2011; Varga et al., 2015; Lei et al., 2016). These studies used TBOA, a non-selective glutamate transport blocker, to mimic the effects of A β on LTP. They also show that a glutamate scavenger system, which works like a sponge to soak up excess glutamate, prevents the A β -induced LTP impairment (Li et al., 2011; Varga et al., 2015). Glutamate clearance is also reduced by A β in a hippocampal synaptosome preparation and when recording STCs in acute brain slices (Li et al., 2009; Scimemi et al., 2013). In addition, GLT-1 expression is reduced due to application of A β , and partial loss of GLT-1 in the APP/PS1 mouse model of AD exacerbates the deficits in hippocampal-dependant memory in these mice (Mookherjee et al., 2011; Scimemi et al., 2013). Together, these data suggest that a reduction in glutamate transporter functionality contributes to the pathophysiology of AD. However, the amount and subtype of glutamate transporter dysfunction required to negatively impact LTP, as well as the underlying mechanisms, remain unknown. To gain a better understanding of LTP impairments in disease, it is necessary to first understand the relationship between glutamate dynamics and LTP, and the precise mechanisms by which poor glutamate clearance can negatively impact LTP; these unknowns are both addressed in the present thesis.

While a reduction in glutamate transporter dysfunction underlying deficits in synaptic plasticity remains an attractive hypothesis in AD, none of these studies have been able to measure glutamate clearance rates at the neuronal surface in real time and *in situ*. Recent work from our lab using iGluSnFR suggests that when GLT-1 is inhibited, the other glutamate transporters can still make significant contributions to glutamate

clearance (Pinky et al., 2018). These results led us to ask what degree of deficit in glutamate clearance is actually required to impair synaptic plasticity.

In my thesis, I provide the first characterization of the relationship between glutamate dynamics and the magnitude of synaptic plasticity. In doing so, I have identified a novel mechanism by which transporter dysfunction leads to an LTP impairment.

1.5 Hypothesis

Deficits in glutamate clearance will cause a significant deficit in LTP. When glutamate clearance is slow enough to impair LTP, this impairment will be due to overaction of extrasynaptic and/or GluN2B-containing NMDARs and downstream activation of intracellular signalling cascades associated with NMDAR-dependent LTD.

1.6 Aims of this thesis project

Aim 1: Characterize the relationship between glutamate dynamics and the magnitude of LTP when glutamate clearance is pharmacologically impaired.

Aim 2: Determine the precise mechanism by which pharmacological inhibition of glutamate transporters can impact LTP with a specific focus on the role of glutamate receptors and intracellular signalling molecules such as GSK3, ERK, calcium and calpains.

Chapter 2 – Methodology

2.1 Animals

One to two-month old male C57BL/6NCrl mice (Charles River, strain code 027) were used except where noted. For a select group of experiments, one to two-month old male FVB/NCrl mice (Charles River, strain code 207) were used. C57BL6 are the most commonly used mouse strain; however, FVBs have been shown to be more susceptible to excitotoxicity (Carulla et al., 2015). Therefore, we wanted to determine whether any major differences in the relationship between glutamate dynamics and LTP exist. Mice had *ad libitum* access to food and water and were housed on a 12h:12h light:dark cycle. All procedures followed the guidelines of the Canadian Council on Animal Care and were approved by Memorial University's Institutional Animal Care Committee.

2.2 Stereotaxic Surgery

To anesthetize the mice, they were placed in an induction chamber with 3% isoflurane. Once unresponsive to toe pinch, they were placed in ear bars of a stereotaxic apparatus (Stoelting) and maintained with 1.5-2% isoflurane. Eye drops were placed in both eyes to prevent them from drying out during the surgical procedure and a subcutaneous injection of the analgesic meloxicam (2 mg/kg in 0.5 mL of 0.9% saline) was administered. The fur was removed from the scalp above bregma and surrounding area. Next, an injection of 0.2% lidocaine was administered below the scalp above bregma and a small incision was made in the same area. Coordinates from bregma to

above hippocampus were measured (2.6 mm posterior, 2.4 mm lateral (right)) and the skull was thinned using a hand drill. The final layer of skull was removed using a bent needle tip to minimize cortical damage. Viral injections of 1 μ L AAV2/1.hSyn.iGluSnFr.WPRE.SV40 (a gift from Loren Looger; Addgene viral prep # 98929-AAV1) for glutamate imaging or 1 μ L AAV1.Syn.GCaMP6f.WPRE.SV40 (a gift from The Genetically Encoded Neuronal Indicator and Effector Project (GENIE) & Douglas Kim; Addgene viral prep # 100837-AAV1) for calcium imaging were administered directly into the hippocampus. AAVs were injected using a Neuros 7002 Hamilton syringe coupled to an infusion pump (Pump 11 Elite Nanomite; Harvard Apparatus) which allowed a constant infusion rate of 2 nL/s. Once the Hamilton syringe was attached to the stereotax, coordinates were remeasured from bregma and the infusion was started just before touching the surface of the brain to prevent the tip from becoming blocked as the syringe tip was lowered into the tissue. The tip was slowly lowered to 1.4 mm ventral to the surface and the syringe was left in place for 5 minutes after the infusion ended to prevent the virus from following up the syringe tract. Once the Hamilton syringe was slowly removed from the brain and the incision was sutured, a subcutaneous injection of 0.5 mL saline was administered to help accelerate recovery. Mice were then placed on a heating pad to recover until they become alert and monitored daily for three days post-surgery and every week afterwards. Mice were scored on a 5-point scale for signs of distress and pain.

2.3 Slice Preparation

Two to five weeks after injection, a range at which iGluSnFR expression remains consistent (Marvin et al., 2013), mice were anesthetized with isoflurane inhalation and brains were quickly removed and placed in oxygenated ice-cold slicing solution containing: 125mM NaCl, 2.5 mM KCl, 25 mM NaHCO₃, 1.25 mM NaH₂PO₄, 2.5 mM MgCl₂, 0.5 mM CaCl₂, and 10 mM glucose. Transverse hippocampal slices (350 μm) were obtained using a Lecia VT1000 Vibratome. Slices were then transferred to a holding chamber containing oxygenated artificial cerebrospinal fluid (ACSF), the same as slicing solution except containing 1 mM MgCl₂ and 2 mM CaCl₂. All sections were allowed to recover for a minimum of 45 minutes at room temperature prior to the start of all imaging experiments or 90 minutes for electrophysiology experiments.

2.4 Real-time Imaging of Glutamate or Calcium Biosensors

Following recovery, slices were transferred to a recording chamber and visualized with an Olympus BX51 microscope. Oxygenated ACSF was continuously perfused at a flow rate of 1-2mL/min and maintained at 24-25 °C with a TC-344C temperature controller (Warner Instruments). Glass pipettes were pulled using a Narishige PB-7 pipette puller to a resistance of 1-3 MΩ and filled with ACSF. The Schaffer collateral pathway was stimulated by controlling an Iso-flex stimulator (A.M.P.I.) with the digital outputs of a Digidata 1550 digitizer (Molecular Devices). iGluSnFR or gCAMP6f responses were evoked by stimulating the Schaffer collateral pathway with either single pulses or TBS. Single pulses were applied with a pulse width of 0.1-0.3 ms and

stimulation intensity of 75-150 μ A. TBS consisted of 10 bursts of 4 pulses at 100 Hz with a 200 ms interburst interval. A pulse width of 0.1 ms and stimulation intensity of 75 μ A was used for TBS. Electrodes were placed at least 50 μ m below the surface of the slice. iGluSnFR or gCaMP6f fluorescence was excited by a LED (Prior, Lumen 300) passing through a 460-490nm bandpass excitation filter. Fluorescence emission was captured through an Olympus 4x/0.28NA objective, filtered through a GFP emission filter (BA510IF) and captured with an EM-CCD camera (Andor, iXon Ultra 897). For real-time imaging, the LED intensity was adjusted to generate a basal fluorescence expression of approximately 10,000 arbitrary units (16-bit scale), the camera's exposure time was set to 0.0047 s, and 4 X 4 binning was used to give 205 Hz imaging. Clampex software was used to trigger LED activation, electrical stimulation and image acquisition. Images were acquired using Andor Solis software.

2.5 Imaging Analysis

Evoked iGluSnFR or GCaMP6f responses were analyzed in ImageJ. For single pulses, a total of 5 stimulus trials (20 second intervals) were averaged together. Between each stimulation trial, a blank trial consisting of LED exposure but no stimulation was acquired. The average of the 5 blank trials was subtracted from the average of the 5 stimulus trials to account for the mild photobleaching observed. Trial averaging and subtraction were performed using the “intrinsic signal processor VSD” plugin for ImageJ. Changes in fluorescence intensity were converted to $\% \Delta F/F$. For TBS, a single stimulation and single blank trial were recorded, to avoid multiple TBS applications to the

same slice. A 10 x 10 pixel (160 x 160 μm) region of interest (ROI) in the stratum radiatum of CA1 (where field recordings would take place for electrophysiology) was used to measure the $\% \Delta F/F$ response. All values were calculated as the average $\% \Delta F/F$ within the ROI for each frame. Using GraphPad Prism, decay tau was analyzed by fitting a non-linear regression single-exponential curve to the iGluSnFR or GCaMP6f response transients, beginning at the response's peak. For single pulses, all frames were included in the analysis. For TBS analysis, decay tau was analysed for each burst so that approximately 40 frames (200 ms post-stimulation) were included in the analysis. Therefore, decay values were capped at 200 ms during TBS.

2.6 Electrophysiology

For electrophysiological recordings of LTP, acute slices were placed in the recording chamber and were left for a minimum of 10 minutes prior to electrode placement. Oxygenated ACSF was continuously perfused at a flow rate of 1-2 mL/min and maintained at 24-25 $^{\circ}\text{C}$ with a TC-344C temperature controller (Warner Instruments). Glass pipettes were pulled using a Narishige PB-7 pipette puller to a resistance of 1-3 $\text{M}\Omega$ and filled with ACSF. The Schaffer collateral pathway was stimulated by controlling an Iso-flex stimulator (A.M.P.I.) with the digital outputs of a Digidata 1550 digitizer (Molecular Devices). Field excitatory postsynaptic potentials (fEPSPs) were evoked by 0.1 ms single pulses generated at a frequency of 0.33 Hz, and the stimulus intensity was adjusted to elicit fEPSPs that were 30-40% of the maximal response. Field potentials were recorded in CA1 stratum radiatum, approximately 400 μm from the site of

stimulation, and signals were amplified and lowpass filtered at 10 kHz with a Multiclamp 700B amplifier (Molecular Devices). Once a stable baseline was established, ACSF containing drugs were applied to the slice for at least 10 minutes prior to LTP induction. LTP was induced using a standard TBS protocol consisting of 10 bursts of 4 pulses at 100 Hz with a 200 msec interburst interval. Recordings continued for 30 or 60 minutes after LTP induction, and LTP magnitude was quantified by averaging the fEPSP slope throughout the last 5 minutes of recording (i.e. 25-30 or 55-60 minutes post-induction). Percent potentiation was expressed as the percentage increase in the average fEPSP slope compared to baseline. All data were collected and analyzed using pClamp10 software (Molecular Devices).

2.7 Immunofluorescence

Acute slices (350 μm) were obtained and maintained in ACSF as described above. Slices were transferred to the recording chamber and perfused (1-2 mL/min) with oxygenated ACSF either with or without 15 μM TBOA. Once stimulating and recording electrodes were placed in the slice as above, a single pulse of stimulation was used to confirm the presence of a clean fEPSP, indicative of a healthy slice. Then slices were stimulated with TBS as above. Slices were transferred to 4% paraformaldehyde either immediately (0 minutes), 10, 20 or 30 minutes following TBS. Control slices were subject to electrode placements and a clean fEPSP evoked by a single pulse was confirmed, but no TBS was administered. Slices remained in 4% paraformaldehyde overnight at 4 $^{\circ}$ C and then transferred to 30% sucrose in 0.01M phosphate buffered saline (PBS) at 4 $^{\circ}$ C

for at least 5 hours. Slices were then flash frozen using liquid nitrogen and sectioned on a cryostat (Leica CM3050 S) to 16 μ M on three alternating slides.

Slide-mounted re-sectioned slices were washed three times using 0.01 M PBS for 5 minutes each and then incubated in blocking solution for 1 hour at room temperature. Blocking solution contained 10% goat serum and 0.4% triton-X 100 in 0.01 M PBS. Slides were then incubated in rabbit anti-pERK primary antibodies (1:500; Cell Signaling Technology; #4370) overnight at 4⁰ C. Primary antibodies were diluted in 0.4% triton-X 100 in 0.01M PBS. After primary antibody incubation, slides were washed three times in 0.01 M PBS and incubated in Alexafluor 594 goat anti-rabbit (1:250; Thermo Fisher Scientific, A-11037) for two hours at RT. Slides were again washed three times with PBS and coverslipped with DAKO fluorescent mounting medium containing DAPI (Abcam; ab104139). All slides were then stored at 4⁰ C until imaging analysis.

2.8 Immunofluorescence Imaging and Analysis

Imaging and analysis were performed similar to a previously described approach (Zhu et al., 2015). Acute slices that were re-sectioned and processed for pERK immunofluorescence were imaged with a Zeiss Axiovert inverted microscope. To obtain clear images of the entire hippocampus while minimizing LED intensity, a 20x/0.8 NA objective lens was used and a 4x4 array of images were tiled and stitched using the Zen Pro software. Images were exported as TIFF files and analyzed in ImageJ. For each acute slice, all re-sectioned images were examined for evidence of clear placements of the stimulating and recording electrodes. pERK intensity was measured in a 100 μ m x 100

μm ROI placed in CA1 stratum radiatum, between the recording and stimulating electrode placements. Mean pERK fluorescence intensity within this ROI was normalized to the background pERK intensity level in an ROI placed in an adjacent, non-stimulated area.

2.9 Drugs

DL-TBOA, DHK, D-APV, AIDA, and MDL 28170 were purchased from Tocris. Ifenprodil tartrate, SB 415286, dantrolene, nifedipine, NASPM and 2-APB were purchased from Sigma Aldrich. (+)-MK 801 maleate was purchased from Thermofisher Scientific. With the exceptions noted below, drugs were bath applied for at least 10 minutes prior to imaging or LTP induction, and bath application continued for at least 10 minutes after LTP induction. For SB 415286, slices were incubated for 1-2 hours prior to LTP induction, and bath application continued for the duration of the experiment (Peineau et al., 2007, 2008). Slices were incubated in (+)-MK-801 for at least three hours prior to transfer to the recording chamber (Nabavi et al., 2013b). AIDA was bath applied for a half hour prior to LTP induction (Kumar and Foster, 2014). MDL 28170 was bath applied starting 10 minutes after LTP induction (Wang et al., 2014).

2.10 Statistical Analysis

All data are represented as mean +/- standard error of the mean (SEM). All statistical analyses were conducted using Graphpad Prism. Since all data were normally distributed, parametric statistics were used throughout. The statistical tests used include: *t*-test, paired

t-test, one-way ANOVA, two-way ANOVA, repeated-measures (RM) two-way ANOVA, and linear regression. The specific statistical test used is listed within the text and/or figure legends. To be considered significant, *p* values <0.05 were used. Reported *n*-values represent the number of acute slices used and for every data set at least three mice were used per group.

Chapter 3 – Results

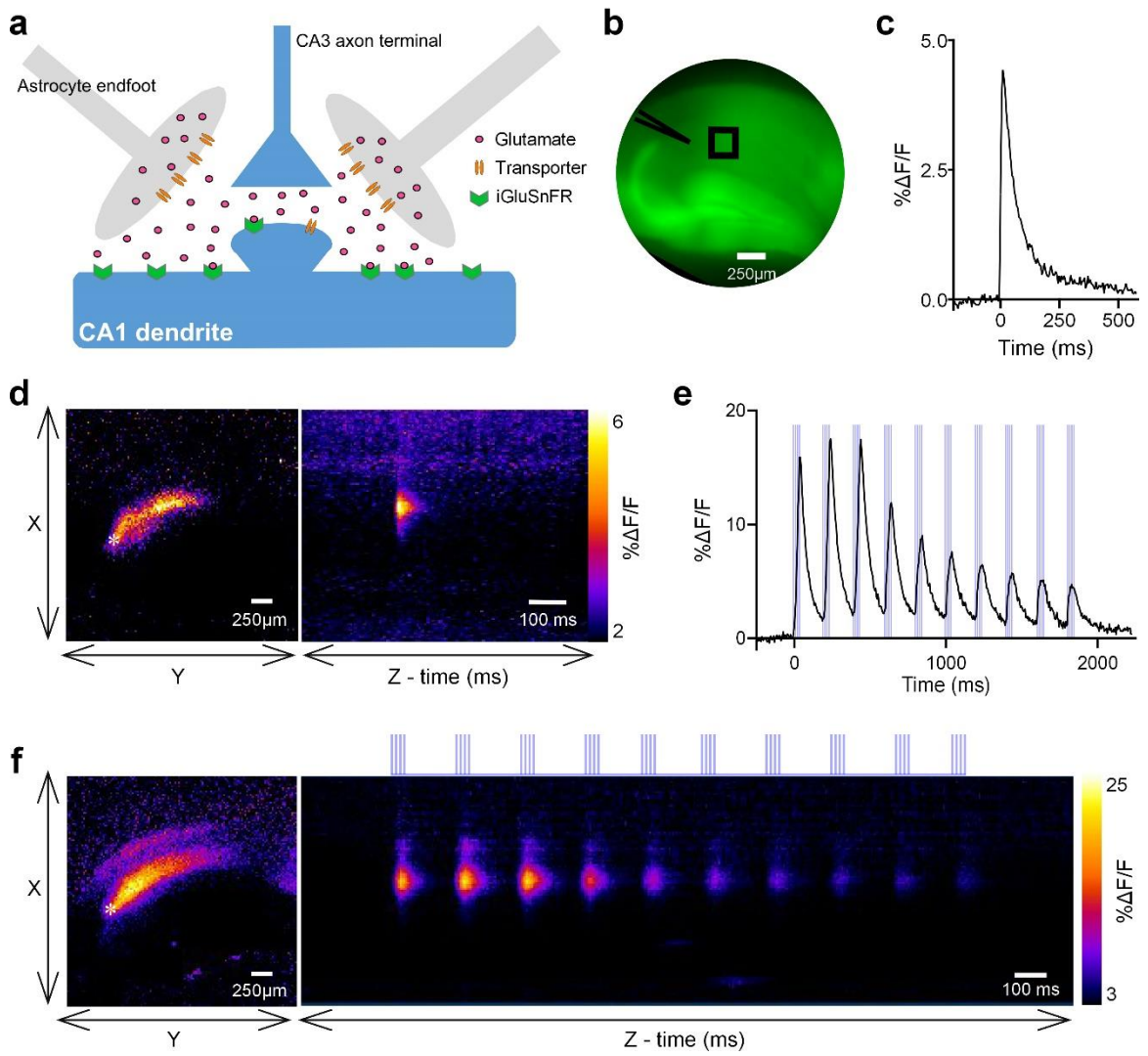
3.1 Visualizing real-time extracellular glutamate dynamics in the hippocampus

Our mechanistic understanding of activity-dependent synaptic plasticity has grown tremendously since the initial discovery of LTP in 1973 (Bliss and Lomo, 1973). It is well-established that NMDAR-dependent plasticity at CA3-CA1 synapses can be bidirectional, and whether LTP or LTD is induced following NMDAR activation depends upon a myriad of factors including the subsequent postsynaptic calcium level and the precise kinases and phosphatases recruited (Shouval et al., 2002; Malenka and Bear, 2004; Connor and Wang, 2016). Interestingly, recent studies suggest that the precise subcellular localization of the activated NMDARs can determine whether LTP or LTD is observed; synNMDAR activation is associated with LTP whereas exNMDAR activation is associated with LTP impairment (Li et al., 2011; Varga et al., 2015), or in some cases, LTD (Papouin et al., 2012; Liu et al., 2013). Despite the relationship between postsynaptic NMDAR localization and synaptic plasticity, very little is known about how the spatiotemporal dynamics of the glutamate that is released during plasticity-inducing stimuli can impact the magnitude and/or direction of subsequent long-term synaptic plasticity. To help understand the influence glutamate dynamics has over activity-dependent plasticity, we visualized extracellular glutamate in real-time using the single-wavelength fluorescent reporter termed iGluSnFR (Marvin et al., 2013). iGluSnFR was virally expressed in the hippocampus under the synapsin promoter (Fig. 2a), allowing us to measure glutamate sensed at the neuronal surface. Endogenous synaptic release was evoked in acute hippocampal slices by electrically stimulating the Schaffer collateral

pathway, and the resultant iGluSnFR transients were captured at 205 frames per second with an EM-CCD camera (Fig. 2b). Rapid iGluSnFR transients with a high signal-to-noise ratio were readily observed following brief electrical stimulation consisting of one pulse (Fig. 2c-d). We then monitored extracellular glutamate dynamics in response to TBS (10 bursts at 5 Hz, each burst consisting of 4 pulses at 100 Hz), a commonly used and physiologically-relevant LTP induction paradigm (Otto et al., 1991). iGluSnFR imaging during TBS revealed 10 clear iGluSnFR peaks corresponding to each burst of the TBS. Glutamate was rapidly cleared from the extracellular space between bursts, and we typically observed a noticeable reduction in the peak $\% \Delta F/F$ of iGluSnFR responses throughout the TBS protocol (Fig. 2e-f).

Figure 2: iGluSnFR expression and responses in hippocampus.

(a) Schematic of a tripartite synapse with iGluSnFR expressed exclusively on neurons. (b) Expression of iGluSnFR in hippocampus with approximate placement of stimulating electrode (narrowing point) and region of interest (square box) to record responses. (c) Representative iGluSnFR response a single pulse of stimulation which can be used to quantify both maximal response and how quickly the response decays. (d) Heat map showing maximal iGluSnFR frame and response profile over time in response to a single pulse of stimulation. Asterisk represents electrode placement. (e) Representative iGluSnFR response to a theta burst induction protocol. Ten distinct peaks are visible indicating the ten different bursts of stimulation given during this protocol. Blue lines represent each individual pulse of stimulation. (f) Heat map showing maximal iGluSnFR frame and response profile over time during theta burst stimulation. Asterisk represents electrode placement.



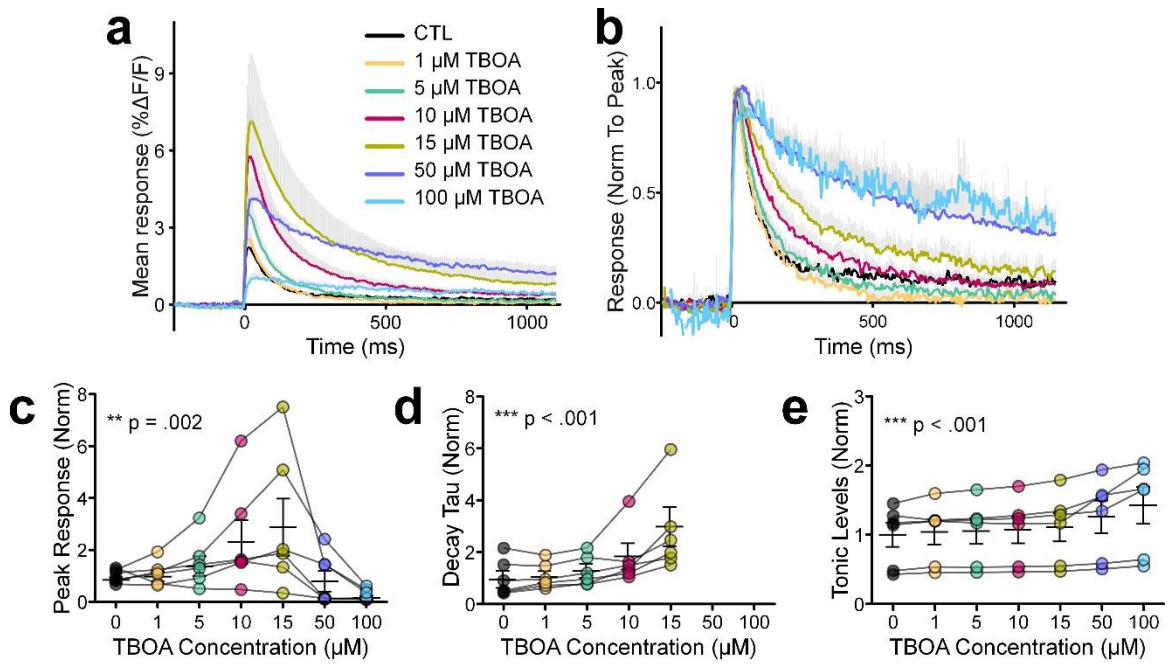
3.2 Non-selective glutamate transporter blockade increases extracellular glutamate accumulation and impairs TBS-LTP

We first used TBOA to investigate the effect of non-selective glutamate transporter inhibition on glutamate dynamics during plasticity induction as well as the strength of TBS-LTP. TBOA bath application from 1-15 μM resulted in a concentration-dependent effect on both the peak and decay tau of iGluSnFR transients evoked by a single pulse (peak: Fig. 3a, c; $n=6$, RM one-way ANOVA, $p=.002$; decay tau: Fig. 3b, d; $n=6$, RM one-way ANOVA, $p<.001$). TBOA concentrations higher than 15 μM (i.e., 50 μM and 100 μM) decreased iGluSnFR peak responses (Fig. 3a, c), consistent with the observation that TBOA concentrations of 50 μM or higher can be toxic to hippocampal neurons (Bonde et al., 2003). In many cases, the iGluSnFR response in 50 or 100 μM TBOA degraded to the point where a decay tau could not be reliably measured; thus, decay kinetics were not quantified for these concentrations. The relative ambient (unstimulated) glutamate level, measured by changes in iGluSnFR basal fluorescence from baseline as described previously (Parsons et al., 2016; Pinky et al., 2018), increased from 1 to 100 μM TBOA as expected (Pinky et al., 2018) (Fig. 3e; $n=6$, RM one-way ANOVA, $p<.001$). As 15 μM TBOA achieved the maximal response on iGluSnFR decay tau values without degrading the response size, we decided to further explore the effect of 15 μM TBOA on both glutamate dynamics during TBS and the magnitude of TBS-LTP one hour post-induction. We also explored the effect of 5 μM TBOA on the same parameters, representing a moderate concentration of TBOA that still exerted an observable effect on evoked iGluSnFR responses.

Figure 3: Blocking all glutamate transporters slows glutamate clearance in a dose dependant manner.

(a) Grouped data to show mean iGluSnFR response to a single pulse of stimulation in the presence of 0, 1, 5, 10, 15, 50, and 100 μM TBOA to visualize the effect on peaks ($n = 6$).

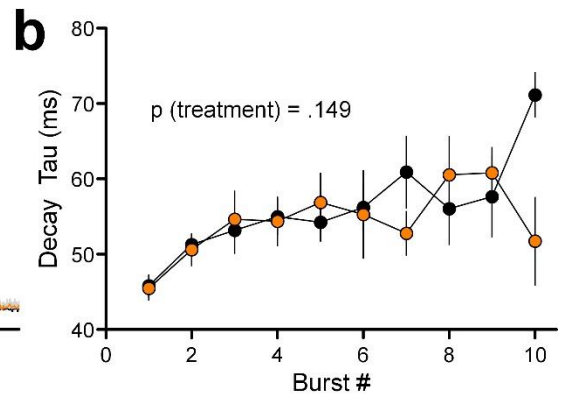
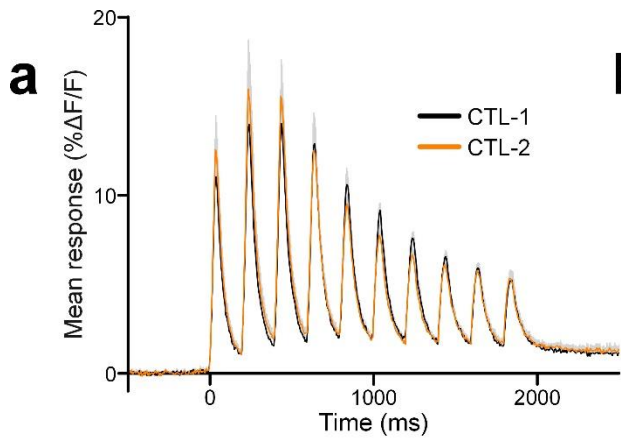
(b) Responses were normalized to peak to visualize the decay of the response within each group. (c, d, e) Peak (c), decay tau (d) and tonic levels (e) of each response were normalized to control to analyze the fold increase in responses. Lines were used to connect paired data. Line and error bars were used to indicate mean \pm S.E.M (RM one-way ANOVA). For decay taus (d), values were not included for 50 and 100 μM because responses were too small to get an accurate measurement.



To determine the effect of TBOA on glutamate dynamics during LTP induction (i.e. TBS), we used TBS to evoke iGluSnFR responses in slices bathed in regular ACSF and then, in the same slice, evoking a second iGluSnFR response with TBS 20 minutes later with bath application of either 5 μ M or 15 μ M TBOA for 10 minutes. This experimental design resulted in paired comparisons for each TBOA concentration. As a control, we found that the iGluSnFR response to the second TBS was not significantly different from the response to the first TBS when the slice was continuously bathed in ACSF (Fig. 4a-b; n=5, RM two-way ANOVA, $p_{(\text{treatment})}=.149$).

Figure 4: Repeated TBS does not alter glutamate clearance rates during subsequent theta bursts.

(a) Grouped data to show mean iGluSnFR response to repeated TBS (n = 6). (b) Decay values were graphed to analyze the effect of repeated theta burst stimulation on glutamate clearance (RM two-way ANOVA).



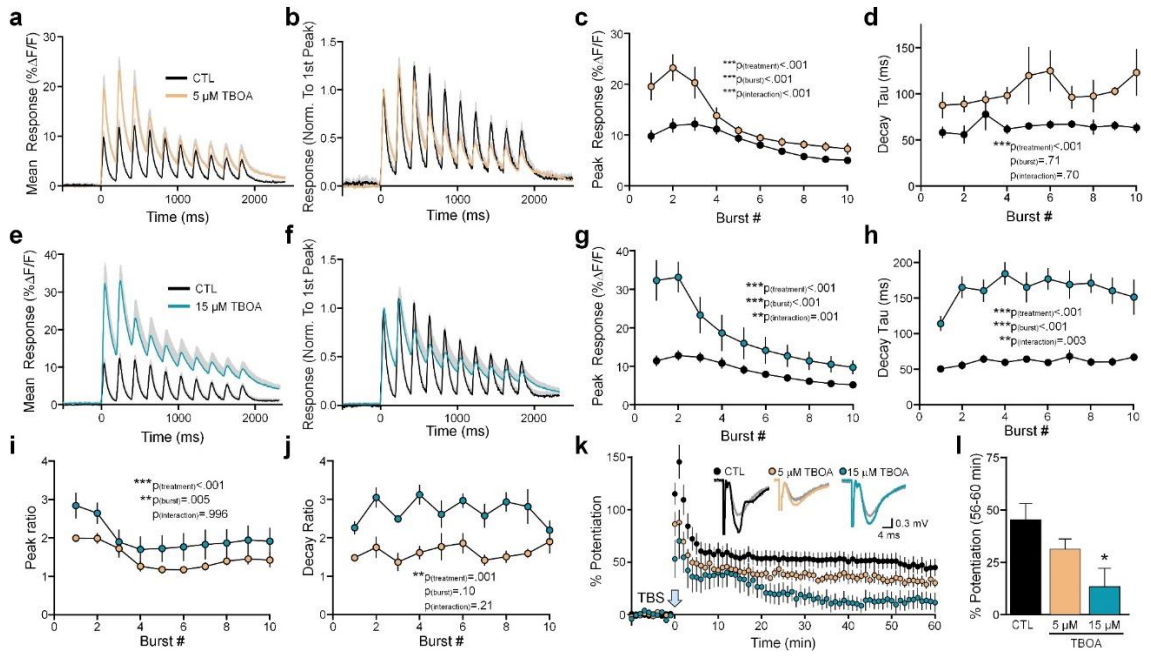
Application of 5 μ M TBOA resulted in a significant increase in the iGluSnFR peaks and decay taus associated with each burst of the TBS (Fig. 5a-d; peak: n=6, RM two-way ANOVA, $p_{(\text{treatment})} < .001$, $p_{(\text{burst\#})} < .001$, $p_{(\text{interaction})} < .001$; decay tau: n=6, RM two-way ANOVA, $p_{(\text{treatment})} < .001$, $p_{(\text{burst\#})} = .706$, $p_{(\text{interaction})} = .700$). Similar effects were observed following application of 15 μ M TBOA (Fig. 5e-h; peak: n=6, RM two-way ANOVA, $p_{(\text{treatment})} < .001$, $p_{(\text{burst\#})} < .001$, $p_{(\text{interaction})} = .001$; decay tau: n=6, RM two-way ANOVA, $p_{(\text{treatment})} < .001$, $p_{(\text{burst\#})} < .001$, $p_{(\text{interaction})} = .003$). The peak ratio, calculated by dividing the peak iGluSnFR response after TBOA by the peak iGluSnFR response before TBOA for each burst, was larger for 15 μ M TBOA than for 5 μ M TBOA (Fig. 5i; n=6 per concentration, RM two-way ANOVA, $p_{(\text{treatment})} < .001$, $p_{(\text{burst\#})} = .005$, $p_{(\text{interaction})} = .996$). The decay tau ratio was also higher for 15 μ M TBOA when compared to 5 μ M TBOA (Fig. 5j; n=6 per concentration, RM two-way ANOVA, $p_{(\text{treatment})} = .001$, $p_{(\text{burst\#})} = .102$, $p_{(\text{interaction})} = .206$). These data indicate that TBOA induces a concentration-dependent slowing of glutamate clearance and increase in extracellular glutamate accumulation during a standard LTP-inducing TBS protocol.

We then used conventional electrophysiology to quantify TBS-LTP in slices bathed in ACSF containing 5 μ M or 15 μ M TBOA. fEPSPs were recorded in CA1 stratum radiatum and LTP was induced by TBS applied to the Schaffer collaterals. TBOA was bath applied for a minimum of 10 minutes prior to TBS and remained in the bath for the duration of the recording. TBOA application resulted in a concentration-dependent impairment of TBS-LTP (Fig. 5k-l: control n=10, 5 μ M TBOA n=6, 15 μ M TBOA n=6, one-way ANOVA, $p = .028$). While the mean %LTP was not significantly different between control and 5 μ M TBOA (Dunnett test vs. control, $p = .361$), post-hoc

significance was observed for 15 μ M TBOA (Dunnett test vs. control, $p=.016$). Together, these data indicate that non-selective inhibition of glutamate transporters promotes extracellular glutamate accumulation during TBS and results in a significant LTP impairment.

Figure 5: Blocking glutamate transporters impairs glutamate clearance and LTP.

(a) Grouped data to show mean iGluSnFR response to theta burst induction protocol before and after 5 μ M TBOA application ($n = 6$). (b) Normalized group data to the first peak to visualize decay after each burst. (c, d) Peak (c) and decay tau (d) values were graphed to analyze the effect of 5 μ M TBOA (RM two-way ANOVA). (e) Grouped data to show mean iGluSnFR response to theta burst induction protocol before and after 15 μ M TBOA application ($n = 6$). (f) Normalized group data to the first peak to visualize decay after each burst. Grey shading (a, b, e, f) represents S.E.M. (g, h) Peak (g) and decay (h) values were graphed to analyze the effect of 15 μ M TBOA (RM two-way ANOVA). (i, j) Peak (i) and decay (j) ratios for 5 μ M and 15 μ M TBOA. Ratios were calculated by dividing the treatment by its own control (two-way ANOVA). (k) LTP in control ($n = 10$), 5 μ M TBOA ($n = 6$) and 15 μ M TBOA ($n = 6$) conditions. (l) Percent potentiation to analyze the effect of 5 μ M and 15 μ M TBOA on LTP (one-way ANOVA, * $p < .05$, Dunnett *post hoc* comparison).

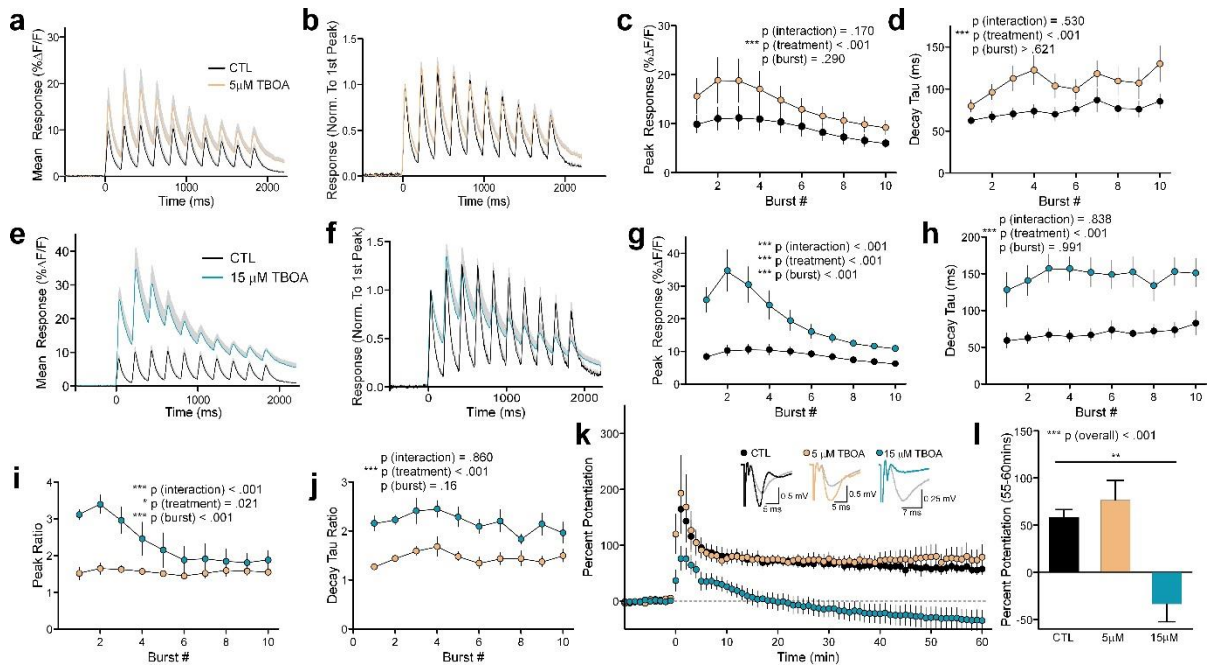


The above data were obtained from C57BL/6 mice, the most widely used inbred mouse strain. To ensure that the relationship between glutamate dynamics and synaptic plasticity was not exclusive to this strain, we repeated the above experiments in FVB/NCrl mice. Similar to what we observed in C57BL/6NCrl mice, TBOA significantly increased iGluSnFR peaks and decay taus for each burst associated with TBS in FVB/NCrl mice (Fig. 6a-j; 5 μ M TBOA peak: n=6, RM two-way ANOVA, $p_{(\text{treatment})} < .001$, $p_{(\text{burst\#})} = .290$, $p_{(\text{interaction})} = .170$; 5 μ M decay tau: n=6, RM two-way ANOVA, $p_{(\text{treatment})} < .001$, $p_{(\text{burst\#})} = .621$, $p_{(\text{interaction})} = .530$; 15 μ M TBOA peak: n=6, RM two-way ANOVA, $p_{(\text{treatment})} < .001$, $p_{(\text{burst\#})} < .001$, $p_{(\text{interaction})} < .001$; 15 μ M decay tau: n=6, RM two-way ANOVA, $p_{(\text{treatment})} < .001$, $p_{(\text{burst\#})} = .991$, $p_{(\text{interaction})} = .838$). As before, peak ratios (Fig. 6i) and decay tau ratios (Fig. 6j) were higher for 15 μ M TBOA compared to 5 μ M TBOA (peak ratio: n=6 per concentration, RM two-way ANOVA, $p_{(\text{treatment})} = .021$, $p_{(\text{burst\#})} < .001$, $p_{(\text{interaction})} < .001$; decay tau ratio: RM two-way ANOVA, $p_{(\text{treatment})} < .001$, $p_{(\text{burst\#})} = .160$, $p_{(\text{interaction})} = .860$). TBOA also impaired TBS-LTP in hippocampal slices from FVB/NCrl mice (Fig. 6k-l; control n=6, 5 μ M TBOA n=6, 15 μ M TBOA n=7, one-way ANOVA, $p < .001$). 5 μ M TBOA had no effect on mean percent potentiation (Dunnett test vs. control, $p = .692$). On the other hand, 15 μ M TBOA resulted in a pronounced LTP deficit in FVB/NCrl mice, with mean fEPSP slope values diminishing below baseline levels within one hour post-induction (Dunnett test vs. control, $p = .003$). Thus, while slight differences in the relationship between glutamate dynamics and synaptic plasticity may exist between strains, these data clearly indicate that in two commonly used mouse strains, impairing glutamate uptake through non-selective glutamate transporter inhibition

negatively impacts TBS-LTP consolidation. All remaining experiments were performed in C57BL6/NCrl mice.

Figure 6: Blocking glutamate transporters impairs glutamate clearance and impairs LTP in FVB mice.

(a) Grouped data to show mean iGluSnFR response to theta burst induction protocol before and after 5 μ M TBOA application ($n = 6$). (b) Normalized group data to the first peak to visualize decay after each burst. (c, d) Peak (c) and decay (d) values were graphed to analyze the effect of 5 μ M TBOA (RM two-way ANOVA). (e) Grouped data to show mean iGluSnFR response to theta burst induction protocol before and after 15 μ M TBOA application ($n = 6$). (f) Normalized group data to the first peak to visualize decay after each burst. (g, h) Peak (g) and decay (h) values were graphed to analyze the effect of 15 μ M TBOA (RM two-way ANOVA). (i, j) Peak (i) and decay (j) ratios for 5 μ M and 15 μ M TBOA. Ratios were calculated by dividing the treatment by its own control (two-way ANOVA). (k) LTP in control ($n = 6$), 5 μ M TBOA ($n = 6$) and 15 μ M TBOA ($n = 7$) conditions. (l) Percent potentiation to analyze the effect of 5 μ M and 15 μ M TBOA on LTP (one-way ANOVA, Dunnett post-hoc test).

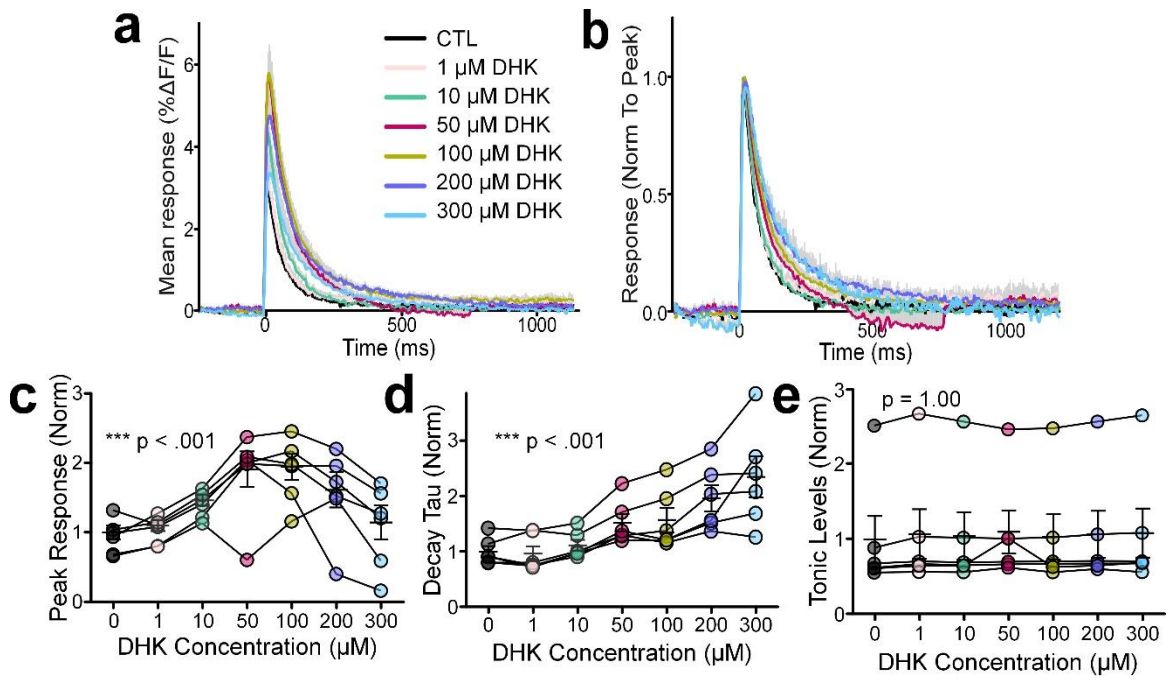


3.3 Selective blockade of GLT-1 slows glutamate clearance but does not impair LTP

Next, we asked whether a similar relationship between glutamate dynamics and synaptic plasticity could be observed following the selective blockade of GLT-1, the brain's most abundant glutamate transporter (Danbolt, 2001). A GLT-1 selective blocker, DHK, resulted in a concentration-dependent increase in the iGluSnFR peak and decay tau in response to a single pulse (Fig. 7a-d; peak: $n=6$, RM one-way ANOVA, $p<.001$; decay tau: $n=6$, RM one-way ANOVA, $p<.001$). Similar to our observations with TBOA, the concentration-dependent increase in iGluSnFR peak began to reverse at higher concentrations; in the case of DHK, concentrations above 100 μM had a negative impact on the peak response (Fig. 7a,c). Unlike TBOA, and in agreement with a previous study from our lab (Pinky et al., 2018), DHK had no significant effect on tonic glutamate levels, as measured by the relative changes in the fluorescence intensity of basal (unstimulated) iGluSnFR (Fig. 7e, $n=6$, RM ANOVA, $p=1.00$). From these concentration-response experiments, we chose to further explore the effects of 50 μM and 100 μM DHK on glutamate dynamics during TBS and the magnitude of TBS-LTP.

Figure 7: Blocking GLT-1 slows glutamate clearance in a dose dependant manner.

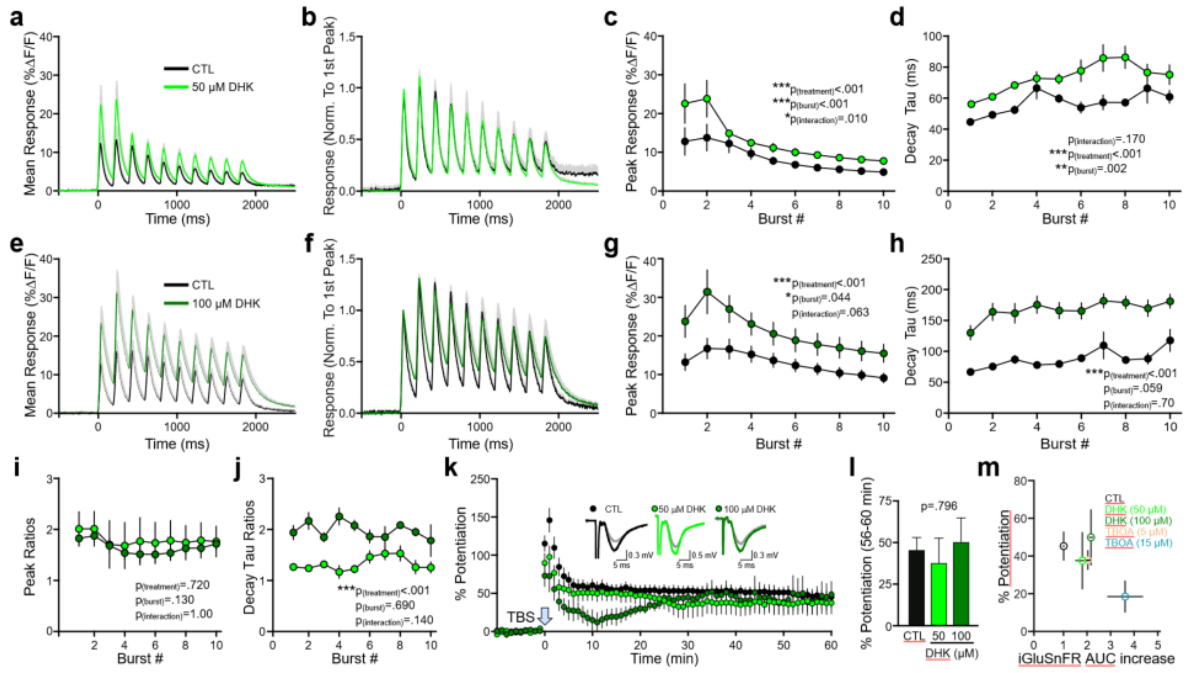
(a) Grouped data to show mean iGluSnFR response to a single pulse of stimulation in the presence of 0, 1, 10, 50, 100, 200 and 300 μ M DHK to visualize the effect on peaks ($n = 6$). (b) Responses were normalized to peak to visualize the decay of the response within each group. (c, d, e) Peak (c), decay tau (d) and tonic levels (e) of each response were normalized to control to analyze the fold increase in responses. Lines were used to connect paired data. Line and error bars were used to indicate mean \pm S.E.M (RM one-way ANOVA).



When bath applied at 50 μ M, DHK resulted in a significant increase in the iGluSnFR peaks and decay taus associated with each burst of the TBS (Fig. 8a-d; peak: n=6, RM two-way ANOVA, $p_{(\text{treatment})} < .001$, $p_{(\text{burst\#})} < .001$, $p_{(\text{interaction})} = .010$; decay tau: n=6, RM two-way ANOVA, $p_{(\text{treatment})} < .001$, $p_{(\text{burst\#})} = .002$, $p_{(\text{interaction})} = .170$). Similar effects were observed following application of 100 μ M DHK (Fig. 8e-h; peak: n=6, RM two-way ANOVA, $p_{(\text{treatment})} < .001$, $p_{(\text{burst\#})} = .044$, $p_{(\text{interaction})} = .063$; decay tau: n=6, RM two-way ANOVA, $p_{(\text{treatment})} < .001$, $p_{(\text{burst\#})} = .059$, $p_{(\text{interaction})} = .700$). While the peak ratios were not significantly different for 50 μ M and 100 μ M DHK (Fig. 8i; n=6 per concentration, RM two-way ANOVA, $p_{(\text{treatment})} = .720$, $p_{(\text{burst\#})} = .130$, $p_{(\text{interaction})} = 1.00$), the decay tau ratio was significantly higher following 100 μ M DHK when compared to 50 μ M DHK (Fig. 8j; n=6 per concentration, RM two-way ANOVA, $p_{(\text{treatment})} < .001$, $p_{(\text{burst\#})} = .690$, $p_{(\text{interaction})} = .140$). Thus, like TBOA, DHK results in slow glutamate clearance and enhances the amount of extracellular glutamate accumulation during a standard TBS protocol. Surprisingly, and in contrast to our TBOA results, we found that these concentrations of DHK did not affect the magnitude of TBS-LTP (Fig. 8k-l; control n=10, 50 μ M DHK n=6, 100 μ M DHK n=6, one-way ANOVA, $p = .796$). By plotting the iGluSnFR area under the curve (fold increase) induced by the various concentrations of DHK and TBOA against the LTP magnitude under the same conditions, it appears that glutamate accumulation during TBS must be increased over 3-fold before a clear effect on LTP consolidation is observed (Fig. 8m).

Figure 8: Blocking GLT-1 slows glutamate clearance during a theta burst protocol without affecting the magnitude of LTP.

(a) Grouped data to show mean iGluSnFR response to TBS induction protocol before and after 50 μM DHK application (n = 6). (b) Normalized group data to the first peak to visualize decay after each burst. (c, d) Peak (c) and decay (d) values were graphed to analyze the effect of 50 μM DHK (RM two-way ANOVA). (e) Grouped data to show mean iGluSnFR response to TBS induction protocol before and after 100 μM DHK application (n = 6). (f) Normalized group data to the first peak to visualize decay after each burst. (g, h) Peak (g) and decay (h) values were graphed to analyze the effect of 100 μM DHK (RM two-way ANOVA). (i, j) Peak (i) and decay (j) ratios for 50 μM and 100 μM DHK. Ratios were calculated by dividing the treatment by its own control (RM two-way ANOVA). (k) LTP in control (n = 10), 50 μM DHK (n = 6) and 100 μM DHK (n = 7) conditions. (l) Percent potentiation to analyze the effect of 50 μM and 100 μM DHK on LTP (one-way ANOVA). (m) Comparison of percent potentiation and iGluSnFR AUC for controls, 50 μM DHK, 100 μM DHK, 5 μM TBOA, and 15 μM TBOA.

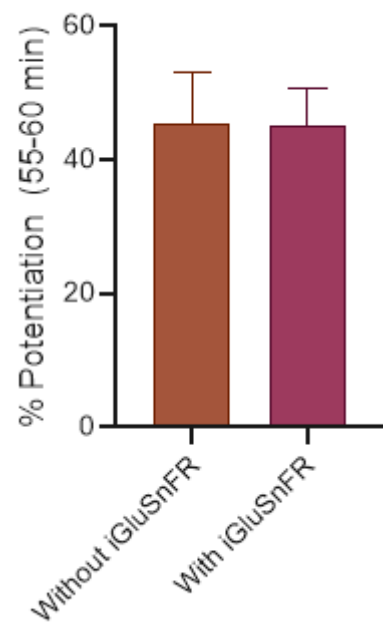


3.4 Variations in glutamate dynamics do not correlate with LTP magnitude in control conditions

As our transporter blocker experiments above suggest that considerable transporter dysfunction is required to exert a negative impact on TBS-LTP, we reasoned that the slice-to-slice variability in glutamate dynamics observed in control conditions would be too insignificant to have any influence over LTP magnitude. To determine whether the natural (i.e., control) variation in glutamate clearance rates correlates with LTP magnitude from one slice to the next, we combined iGluSnFR imaging with conventional electrophysiological recordings in the same experiments. Importantly, iGluSnFR expression does not significantly alter the magnitude of potentiation (Fig 9. $n_{(\text{without iGluSnFR})}=10$, $n_{(\text{with iGluSnFR})}=15$, unpaired t-test, $p=0.996$).

Figure 9: The presence of iGluSnFR in the hippocampus does not significantly alter the magnitude of potentiation post LTP induction.

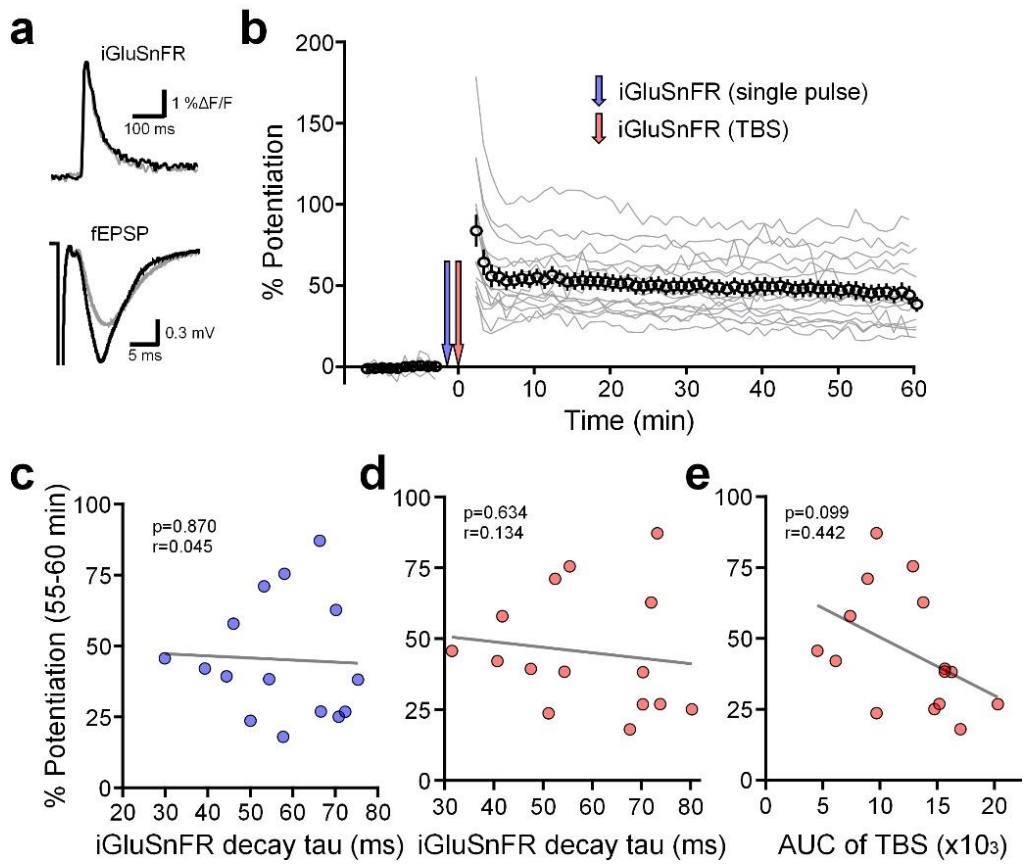
The magnitude of potentiation was compared in slices with (n=15) and without (n=10) iGluSnFR expression (unpaired t-test, p=0.996).



First, a stable baseline was established by the fEPSP slope. The iGluSnFR response to a single pulse was then captured prior to LTP induction, and we also captured the iGluSnFR response during LTP induction with TBS. fEPSPs were then recorded every 20 seconds for 60 minutes post-induction in the same slices. If synaptic plasticity exhibits a high sensitivity to glutamate clearance kinetics during TBS, we should observe the weakest LTP in slices that cleared glutamate the slowest during LTP induction. In response to a single pulse, iGluSnFR decay taus varied from 30 ms to 75 ms; however, there was no significant correlation between iGluSnFR decay tau and LTP magnitude (Fig. 10c, $n=15$, $p=.870$). Similarly, LTP magnitude did not correlate with glutamate dynamics during TBS under control conditions, as quantified by both the decay tau after the first burst (Fig. 10d, $n=15$, $p=.630$) or the area under the curve of the iGluSnFR response to the full TBS (Fig. 10e, $n=15$, $p=.099$). This area measurement reflects the relative amount of extracellular glutamate accumulation throughout the entire TBS, and while slices with larger iGluSnFR areas tended to have weaker LTP, this trend did not reach statistical significance. These experiments indicate that LTP strength is not significantly affected by the 2.5-fold variation in glutamate dynamics we observed in control conditions. Together with our findings with TBOA and DHK, our data indicate that considerable impairments in transporter-mediated glutamate uptake are required before a detrimental effect on TBS-LTP can be observed.

Figure 10: Natural variation in glutamate clearance is not associated with variability in percent potentiation.

(a) Representative traces from single iGluSnFR responses (top) and fEPSP responses (bottom) before (grey) and one hour after (black) theta burst stimulation. (b) Experimental design showing the combination of LTP and iGluSnFR. Gray traces represent individual experiments ($n = 15$). (c, d) Correlation of decay tau for a single pulse (c) and the first burst of a theta burst (d) with the magnitude of potentiation at the end of the experiment. (e) Area of the iGluSnFR response to TBS (area under the curve; AUC) correlated with percent potentiation.



3.5 Glutamate transporter inhibition does not impair LTP through excessive activation of NMDARs or recruitment of common LTD pathways

Next, we sought to determine the precise mechanism by which glutamate transporter dysfunction impairs LTP. By altering the spatiotemporal dynamics of extracellular glutamate during LTP-inducing stimuli, it is possible that 15 μ M TBOA promotes the simultaneous activation of intracellular signaling associated with LTP and LTD that oppose each other. To determine whether the excessive glutamate accumulation during 15 μ M TBOA-TBS activated an NMDAR-independent LTD pathway to oppose LTP consolidation, we blocked NMDARs with the competitive antagonist D-APV (50-100 μ M). In the presence of D-APV, TBS-LTP was significantly impaired as expected (Larson and Lynch, 1988). However, LTD was not revealed in the presence of both D-APV and TBOA, suggesting that TBOA is unlikely to recruit NMDAR-independent LTD during TBS (Fig. 11a-b, control n=10, D-APV n=6, D-APV+TBOA n = 6; one-way ANOVA, p=.005; post-hoc Tukey tests: control vs. D-APV p=.021, control vs. D-APV+TBOA p=.010, D-APV vs. D-APV+TBOA p=.947). In agreement, the TBOA-induced LTP impairment was not due to the activation of group 1 mGluR-mediated LTD (Huber and Luscher, 2010), as the mGluR1 antagonist AIDA (200 μ M) was unable to restore TBOA-LTP to control levels (Fig. 11c-d; control n=10, AIDA n=7, AIDA+TBOA n = 6; one-way ANOVA, p=.009; post-hoc Tukey tests: control vs. AIDA p=.992, control vs. AIDA+TBOA p=.011, AIDA vs. AIDA+TBOA p=.023). Furthermore, paired-pulse ratio experiments indicate that TBOA-TBS did not result in a presynaptically-expressed LTD (Fig. 11e; n=7; paired t-test; p=.169). Similar results to our D-APV experiments were obtained with the NMDAR pore-blocker, MK-801 (100 μ M; Fig. 11f-g; control

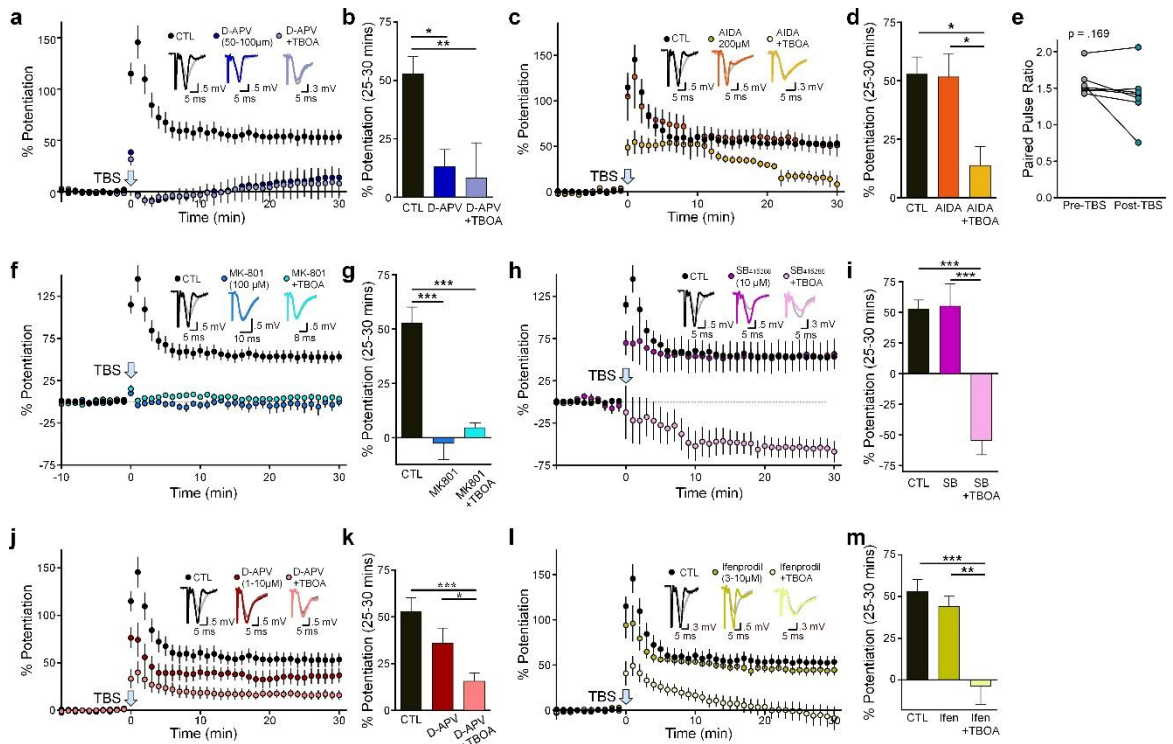
n=10, MK-801 n=7, MK-801+TBOA n=6, one-way ANOVA, $p < .001$; post-hoc Tukey tests: control vs. MK-801 $p < .001$, control vs. MK-801+TBOA $p < .001$, MK-801 vs. MK-801+TBOA $p = .765$). As MK-801 preserves the glutamate binding domain of NMDARs, this result also indicates that the TBOA-LTP impairment does not result from the recruitment of metabotropic NMDAR LTD (Nabavi et al., 2013b). Likewise, inhibition of GSK-3, a kinase known to play a critical role in NMDAR-dependent LTD (Peineau et al., 2007; Jo et al., 2011; Bradley et al., 2012), was also unable to restore TBOA-LTP to control levels (Fig. 11h-i, control n=10, SB n=7, SB+TBOA n=7; one-way ANOVA $p < .001$; post-hoc Tukey tests: control vs. SB $p = .990$, control vs. SB+TBOA $p < .001$, SB vs. SB+TBOA $p < .001$). In fact, while SB415286 (10 μM) had no effect on LTP on its own, TBS induced a clear LTD when GSK-3 was inhibited in the presence of TBOA.

Excessive activation of NMDARs can have a detrimental effect on LTP (Katagiri et al., 2001). However, to our surprise, we were unable to restore TBOA-LTP to control levels by using sub-saturating concentrations (1-10 μM) of D-APV. No differences were observed between D-APV concentrations within this range, and the data were pooled (Fig. 11j-k, control n=10, D-APV_(1-10 μM) n=14, D-APV_(1-10 μM)+TBOA n=23; one-way ANOVA, $p < .001$; post-hoc Tukey tests; control vs. D-APV_(1-10 μM) $p = .220$, control vs. D-APV_(1-10 μM)+TBOA $p < .001$, D-APV_(1-10 μM) vs. D-APV_(1-10 μM)+TBOA $p = .043$). Ifenprodil (3/10 μM), the GluN2B-containing NMDAR antagonist was also unable to restore TBOA-LTP to control levels (Fig. 11l-m; ifenprodil n=10; ifenprodil + TBOA n=12, one-way ANOVA, $p < .001$; post-hoc Tukey tests; control vs. ifenprodil $p = .783$, control vs. ifenprodil+TBOA $p < .001$, ifenprodil vs. ifenprodil+TBOA $p = .002$), suggesting that

excessive activation of GluN2B-containing NMDARs cannot account for the LTP impairment observed in the present study.

Figure 11: TBOA induced LTP impairment is not mediated by NMDAR overactivation or recruitment of common LTD pathways.

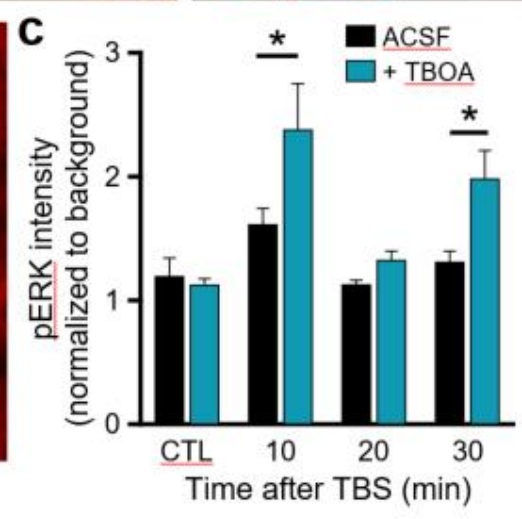
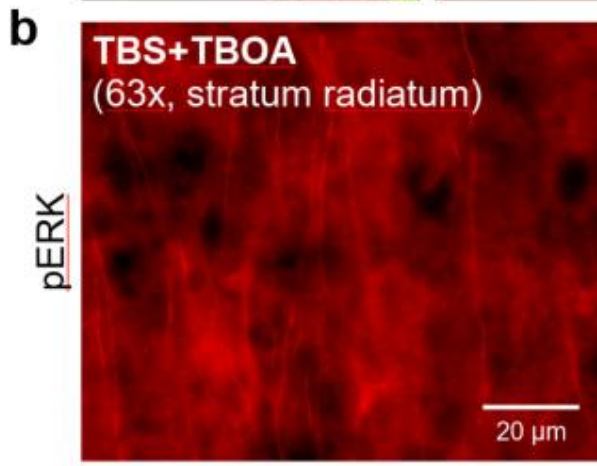
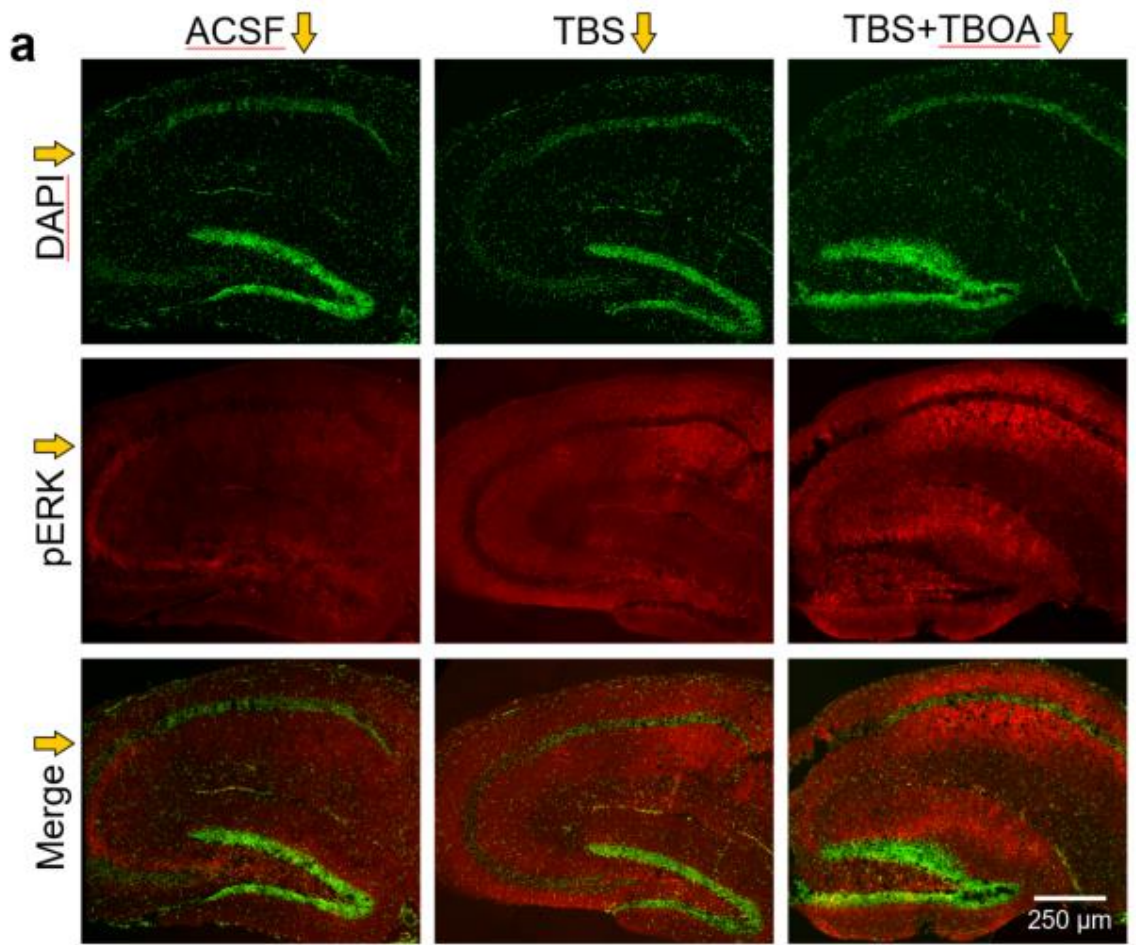
(a, b) LTP in controls ($n = 10$) and in the presence of a saturating concentration of D APV (blocks all NMDARs; 50-100 μM) alone ($n = 6$) or with 15 μM TBOA ($n = 6$). (b) Percent potentiation (one-way ANOVA). (c, d) LTP in controls ($n = 10$) and in the presence of 200 μM AIDA (blocks mGluR1) alone ($n = 7$) or with 15 μM TBOA ($n = 6$). (d) Percent potentiation (one-way ANOVA). (e) Paired pulse ratio before theta burst stimulation and 30 minutes after LTP induction in the presence of 15 μM TBOA. Pulses were given 50 msec apart ($n = 7$; paired t -test). (f, g) LTP in controls ($n = 10$) and in the presence of 100 μM MK-801 (blocks NMDAR pore) alone ($n = 7$) or with 15 μM TBOA ($n = 6$). (g) Percent potentiation (one-way ANOVA). (h, i) LTP in controls ($n = 10$) and in the presence of 10 μM SB415286 (inhibits GSK 3beta) alone ($n=7$) or with 15 μM TBOA ($n = 7$) conditions. (i) Percent potentiation (one-way ANOVA). (j, k) LTP in controls ($n = 10$) and in the presence of a low concentration of D APV (blocks all NMDARs; 1-10 μM) alone ($n = 14$) or with 15 μM TBOA ($n = 23$). (k) Percent potentiation (one-way ANOVA). (l, m) LTP in controls ($n = 10$) and in the presence of 3/10 μM ifenprodil (blocks GluN2B-containing NMDARs) alone ($n = 10$) or with 15 μM TBOA ($n = 12$). (m) Percent potentiation (one-way ANOVA).



These results suggesting that excessive activation of GluN2B-containing NMDARs cannot account for the LTP impairment were surprising given the previously reported links between glutamate spillover, exNMDAR overactivation and synapse weakening (Katagiri et al., 2001; Li et al., 2009, 2011; Varga et al., 2015). Therefore, to further probe the possible involvement of excessive NMDAR activity in the TBOA-LTP impairment, we fixed acute slices 10 minutes following TBS, re-sectioned them to 16 μm on a cryostat and quantified pERK immunofluorescence levels in CA1 stratum radiatum. pERK is an essential kinase for TBS-LTP (Zhu et al., 2015) but is inactivated by high levels of exNMDAR (Ivanov et al., 2006) or GluN2B-containing NMDAR (Myung et al., 2005) stimulation. Thus, if exNMDAR and/or GluN2B-containing NMDAR overactivation mediates the TBOA-LTP impairment, we would expect to see a reduction in the TBS-induced recruitment of pERK in slices treated with TBOA. The mean pERK fluorescence intensity was transiently elevated by TBS as previously reported (Wang et al., 2014); however, pERK levels increased even higher following TBS in TBOA-treated slices, with significant post-hoc differences identified both 10- and 30-minutes post-TBS (Fig. 12; $n=4-6$ slices per time per condition; two-way ANOVA, $p_{(\text{treatment})}=0.005$, $p_{(\text{time})}<.001$, $p_{(\text{interaction})}=0.106$; post-hoc Bonferroni tests comparing TBS vs. TBS+TBOA; 0 minutes $p>.05$, 10 minutes $p=.023$, 20 minutes $p>.05$, 30 minutes $p=.040$). This pERK hyperactivation argues against the overactivation of exNMDARs or GluN2B-containing NMDARs in the present conditions.

Figure 12: pERK is increased post-LTP induction in the presence of 15 μ M TBOA.

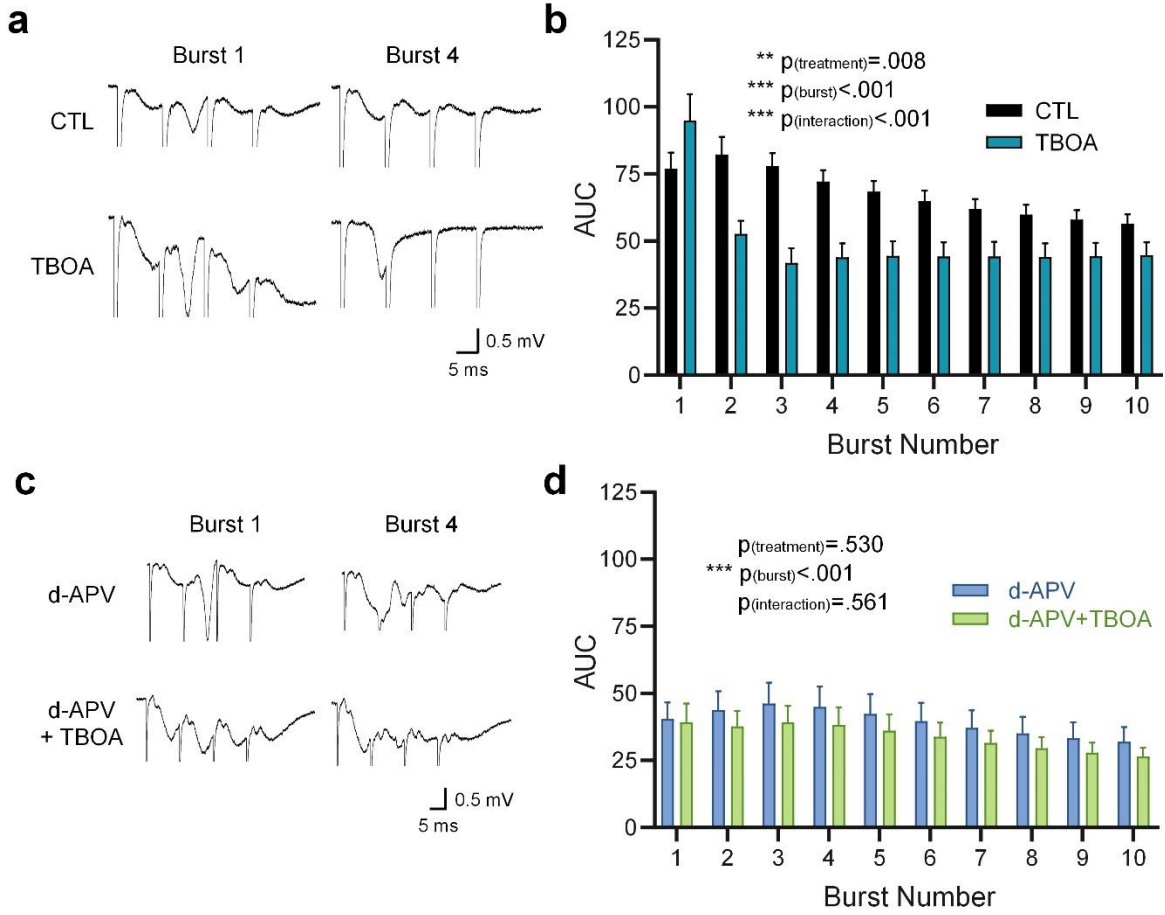
(a) Representative images of pERK (red) and DAPI (pseudocolored green for clarity) in slices without TBS, with TBS, and with TBS and 15 μ M TBOA. **(b)** Representative image showing that pERK staining is throughout the dendrites in the stratum radiatum. **(c)** pERK intensity quantified in the stratum radiatum of CA1 (two-way ANOVA).



As extracellular glutamate accumulation during TBS is enhanced over three-fold in the presence of 15 μ M TBOA (see Fig. 7m), we reasoned that instead of a pathological overactivation, perhaps NMDARs rapidly desensitize during TBOA-TBS. To test this possibility, we calculated the area under the curve of the fEPSP response to each of the ten bursts associated with the TBS train. Compared to control slices, TBOA did not alter the mean fEPSP area during the first burst; however, this was followed by a significant reduction in fEPSP area during subsequent bursts (Fig. 13a,b, control n=14, TBOA n=9; RM two-way ANOVA, $p_{(\text{treatment})}=.008$, $p_{(\text{burst\#})}<.001$, $p_{(\text{interaction})}<.001$; post-hoc Bonferroni tests for control vs. TBOA: burst #2 $p=.017$, burst #3 $p=.001$, burst #4 $p=.005$, burst #5 $p=.026$, all other bursts $p>.05$). The dampening effect of TBOA on the postsynaptic response to TBS was both mimicked and occluded by pre-treatment with D-APV (Fig. 13c-d, D-APV n=6, D-APV+TBOA n=6, RM two-way ANOVA, $p_{(\text{treatment})}=.530$, $p_{(\text{burst\#})}<.001$, $p_{(\text{interaction})}=.561$; post-hoc Bonferroni tests for D-APV vs. D-APV+TBOA: all bursts $p>.05$). Together, our data provide a strong argument that the TBS-LTP deficit observed following transporter inhibition is not mediated by a pathological overactivation of NMDARs. In fact, our electrophysiological findings here suggest that the NMDAR component of the postsynaptic population response to TBS is significantly reduced in the presence of TBOA.

Figure 13: Impaired glutamate clearance causes desensitization of NMDARs during theta burst stimulation.

(a, c) Representative electrophysiology traces of bursts 1 and 4 within TBS. (b) Area of each burst during theta burst stimulation in control (n = 14) and 15 μ M TBOA (n = 9) conditions (RM two-way ANOVA). (d) Area of each burst during TBS n in the presence of 50-100 μ M D APV alone (n = 6) or with 15 μ M TBOA (n = 6) conditions (RM two-way ANOVA).

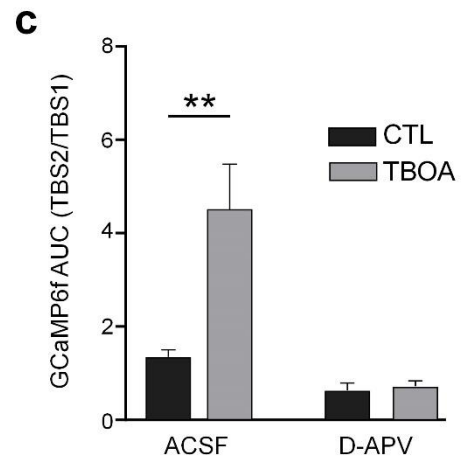
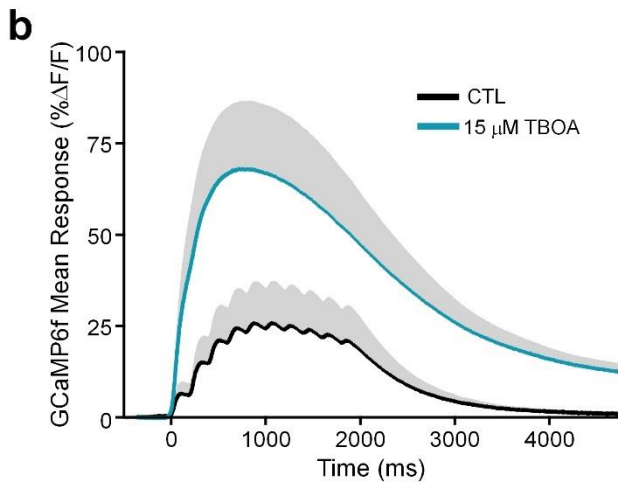
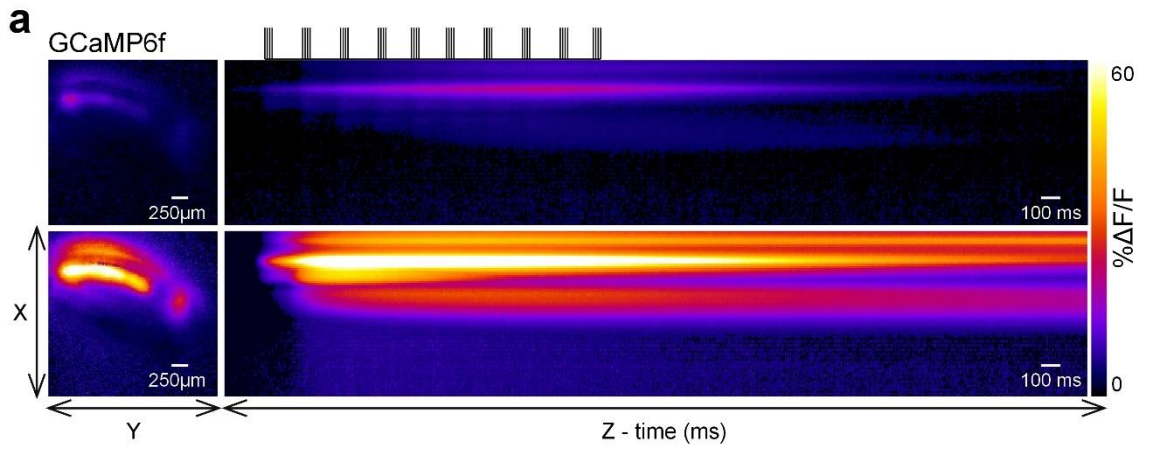


3.6 Glutamate transporter inhibition impairs LTP by activation of L-type voltage gated calcium channels and calpain

Calcium influx through NMDARs is required for TBS-LTP at the CA3-CA1 synapse. Considering our finding that the fEPSP response to TBS is reduced by glutamate transporter inhibition, we next quantified the intracellular calcium response to TBS in control conditions and in the presence of 15 μ M TBOA. These experiments were paired, in that each slice was initially subjected to TBS in ACSF, left to rest for 10 minutes followed by a 10-minuted bath application of TBOA (15 μ M), and a second TBS was evoked. To quantify the effect of TBOA, the area under the curve of the GCaMP6f response to the second TBS was divided by that to the first TBS; these data are expressed in Fig. 14 as “GCaMP6f AUC (TBS2/TBS1)”. As we reasoned that the calcium influx associated with the second TBS may be influenced by the synaptic changes induced by the first TBS, these data were compared to control slices that also received two TBS trains separated by 20 minutes, but ACSF alone (i.e., no TBOA) was bathed continuously throughout the experiment. Indeed, in control slices, the area under the curve of the GCaMP6f response the second TBS was 1.35 (\pm 0.16)-fold greater than the response to the first TBS (Fig. 14). However, in TBOA-treated slices, the fold GCaMP6f response increased to 4.51 (\pm 0.97), a value significantly higher than control slices. D-APV completely prevented the TBOA-induced increase in intracellular calcium evoked by TBS (Fig 14, n= 6-7 per condition; two-way ANOVA; $p_{(TBOA)}=.004$; $p_{(D-APV)}<.001$; $p_{(interaction)}=.010$, post-hoc Bonferroni tests for ACSF vs. TBOA: without D-APV $p<.001$, with D-APV $p>.05$), suggesting that the excess calcium response is at least initially dependent on NMDAR activation.

Figure 14: The presence of 15 μM TBOA during theta burst stimulation increases post-synaptic calcium which requires activation of NMDARs.

(a) Heat map showing maximal GCaMP6f frame and response profile through time during theta burst stimulation in control (top panel) and 15 μM TBOA (bottom panel). (b) Grouped data to show mean GCaMP6f response to theta burst induction protocol before and after 15 μM TBOA application ($n = 6$). (c) Ratio of the area under the curve during the second theta burst over the first. The second theta bursts were all performed in the presence or absence of 15 μM TBOA and/or 100 μM D APV ($n = 6$ per group; two-way ANOVA).



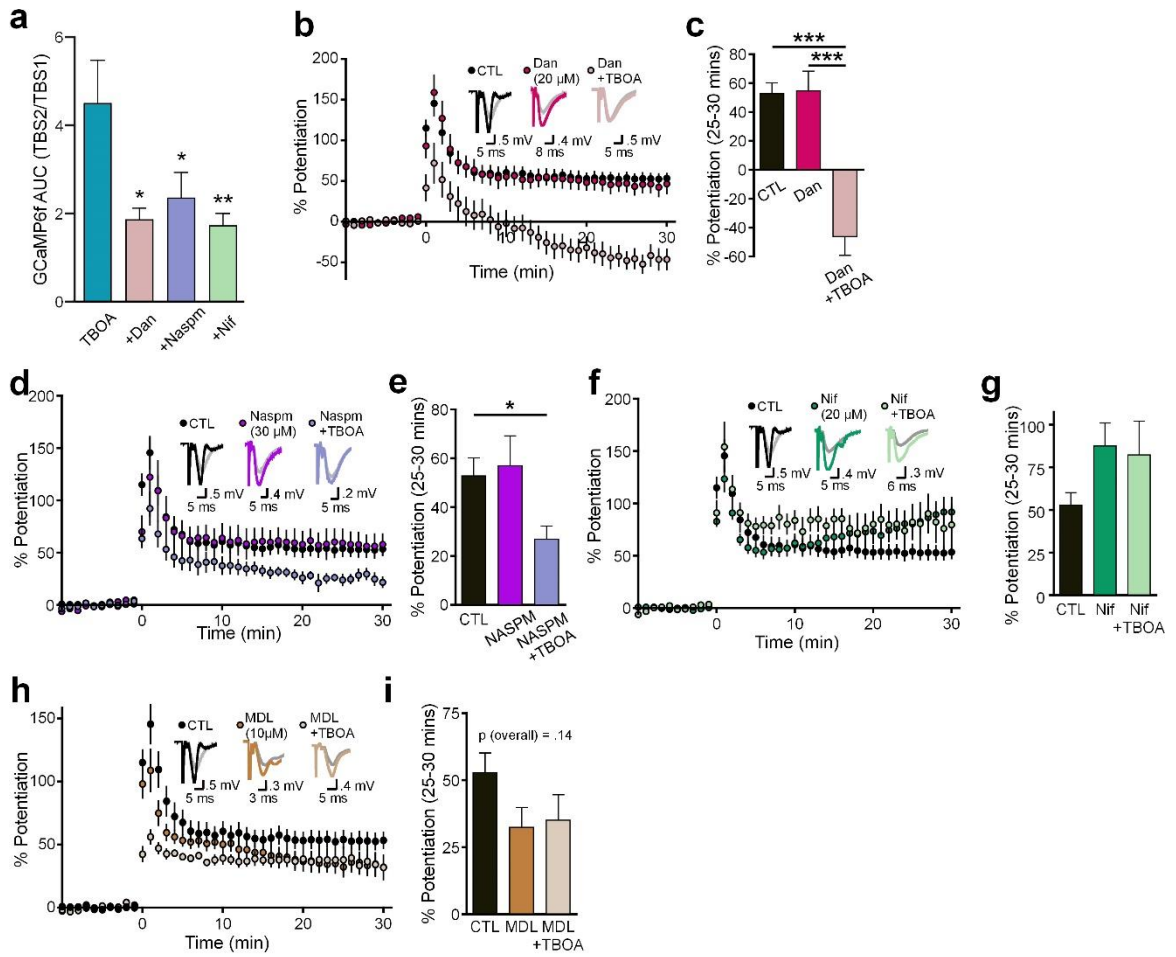
In the presence of TBOA, the NMDAR-mediated component of the fEPSP rapidly diminishes by the second burst of TBS. Thus, we reasoned that another source of calcium, one that is downstream of NMDAR activation, must contribute the dramatic effect of TBOA on the calcium response to TBS. We used dantrolene (20 μ M), Nasp_m (30 μ M) and nifedipine (20 μ M) to assess the putative contribution of intracellular calcium stores, GluA2-lacking AMPARs and L-type voltage-gated calcium channels (L-VGCCs) to the excessive cytosolic calcium levels obtained during TBOA-TBS, respectively. Interestingly, all compounds were able to decrease the mean effect of TBOA on the total GCaMP6f area during TBS, suggesting the contribution of multiple calcium sources to TBOA-TBS (Fig. 15a, n=6 per group, one-way ANOVA, p=.012, post-hoc Dunnett tests vs. TBOA alone: dantrolene+TBOA p=.013, Nasp_m+TBOA p=.047, nifedipine+TBOA p=.009). We then assessed whether either of these compounds alone could prevent the inhibition of LTP induced by TBOA. Interestingly, dantrolene had no effect on LTP in the absence of TBOA, but resulted in robust LTD when co-applied together with TBOA (Fig. 15b-c, control n=10, dantrolene n=6, dantrolene+TBOA n=6; one-way ANOVA, p<.001; post-hoc Tukey tests: control vs. dantrolene p=.988, control vs. dantrolene+TBOA p<.001, dantrolene vs. dantrolene+TBOA p<.001). Nasp_m also had no effect on LTP when applied on its own, but was unable to prevent the inhibitory effect of TBOA on LTP consolidation (Fig. 15d-e, control n=10, NASPM n=4, Nasp_m+TBOA n=7; one-way ANOVA, p=.033, post-hoc Tukey tests: control vs. Nasp_m p=.938, control vs. Nasp_m+TBOA p=.048, Nasp_m vs. Nasp_m+TBOA p=.075). In contrast, nifedipine, completely prevented the degradative effect of TBOA on LTP (Fig. 15f-g, control n=10, nifedipine n=6, nifedipine+TBOA n=8, one-way ANOVA p=.166; post-hoc Tukey tests:

control vs. nifedipine $p=.219$, control vs. nifedipine+TBOA $p=.271$, nifedipine vs. nifedipine+TBOA $p=.965$). Thus, while multiple calcium sources contribute to the calcium overload during TBOA-TBS, calcium entry through L-VGCCs is required for the plasticity impairment induced by glutamate transporter inhibition.

The calcium-dependent proteases calpain-1 and calpain-2 have received much recent attention for their opposing roles in synaptic plasticity (Baudry and Bi, 2016). Calpain-2 has been shown to act as a molecular brake that can limit the magnitude of TBS-LTP during the maintenance phase (Wang et al., 2014). Interestingly, calpain-2 can be activated by pERK (Glading et al., 2004; Chen et al., 2010) as well as millimolar concentrations of cytosolic calcium (Baudry and Bi, 2016). As TBOA-TBS resulted in both pERK hyperactivity and elevated cytosolic calcium, we hypothesized that calpain-2 recruitment could be acting as an LTP brake under these conditions. To test this hypothesis, we induced TBS-LTP in the presence or absence of TBOA, and bath applied the calpain inhibitor MDL-28170 (10 μ M) 10 minutes after LTP induction. This delayed application strategy was used in a previous study to inhibit calpain-2's effect on LTP consolidation without interfering with calpain-1's effect on LTP induction (Wang et al., 2014). We found that MDL-28170 completely prevented the TBOA-induced LTP impairment (Fig 15h-i, control $n=10$, MDL $n=6$, MDL+TBOA $n=6$, one-way ANOVA $p=.142$, post-hoc Tukey tests: control vs. MDL $p=.246$, control vs. MDL+TBOA $p=.201$, MDL vs. MDL+TBOA $p=.993$).

Figure 15: The presence of 15 μ M TBOA during TBS increases post-synaptic calcium via influx through VGCC to impair LTP.

(a) Ratio of the area under the curve during the second theta burst over the first were calculated. The second theta bursts were all performed in the presence of 15 μ M TBOA and normal ACSF ($n = 6$), 20 μ M Dantrolene (Dan; blocks ryanodine receptors; $n = 6$), 30 μ M Naspn (blocks GluA2-lacking AMPARs; $n = 6$) or 20 μ M Nifedipine (Nif; blocks L-type VGCCs; $n = 6$; one-way ANOVA). (b, c) LTP in controls ($n = 10$) and in the presence of Dantrolene alone ($n = 6$) or with 15 μ M TBOA ($n = 6$). (c) Percent potentiation (one-way ANOVA). (d, e) LTP in controls ($n = 10$) and in the presence of Naspn alone ($n = 4$) or with 15 μ M TBOA ($n = 7$). (e) Percent potentiation (one-way ANOVA). (f, g) LTP in controls ($n = 10$) and in the presence of Nifedipine alone ($n = 6$) or with 15 μ M TBOA ($n = 8$). (g) Percent potentiation (one-way ANOVA). (h, i) LTP in controls ($n = 10$) and in the presence of 10 μ M MDL28170 (inhibits calpain activity) alone ($n = 6$) or with 15 μ M TBOA ($n = 6$). (i) Percent potentiation (one-way ANOVA).



Chapter 4 – Discussion

Synaptic and/or GluN2A-containing NMDARs are believed to initiate LTP while extrasynaptic and/or GluN2B-containing NMDARs are believed to initiate LTD (Steigerwald et al., 2000; Groc et al., 2006; Hardingham and Bading, 2010; Paoletti et al., 2013). Since glutamate transporter dysfunction underlying deficits in LTP observed in many neurodegenerative diseases is an attractive and well cited hypothesis (Li et al., 2009, 2011; Mookherjee et al., 2011; Scimemi et al., 2013; Tu et al., 2014; Varga et al., 2015; Lei et al., 2016), it is important to understand how extracellular glutamate dynamics affect synaptic plasticity. Here, we characterized the relationship between glutamate clearance using iGluSnFR and conventional electrophysiology. When glutamate clearance is slow enough to impair LTP, we determined the underlying mechanism. During slow glutamate clearance, the LTP impairment was not due to activation of NMDAR-dependent LTP pathway or overactivation of NMDARs. Surprisingly, the LTP impairment due to TBOA resulted from a reduction in current influx through NMDARs and an increase in intracellular calcium via L-type VGCCs. This pathological increase in calcium and a simultaneous increase in pERK activate calpains to impair LTP.

4.1 Three-fold deficits in glutamate clearance are required to impair synaptic plasticity

Reductions in glutamate transporters have been associated with a deficit in LTP (Li et al., 2009, 2011; Varga et al., 2015; Lei et al., 2016). Here, we found that the clearance of glutamate rates must be slowed three-fold with TBOA before a deficit in the magnitude of LTP is observed. Many studies report a 13-30% deficit in glutamate clearance in animal models of AD (Li et al., 2009; Liu et al., 2016a). However, here we show that with 100 μ M DHK, the GLT-1 selective antagonist, total glutamate clearance is slowed two-fold; yet the magnitude of LTP remains unaffected. A 40% reduction in surface expression of GLT-1 due to amyloid-beta application was shown to reduce glutamate clearance two-fold with STCs and believed to contribute to the LTP impairment (Scimemi et al., 2013). However, the authors found that both monomers and oligomers of amyloid beta slow glutamate clearance while others have shown that only oligomers impair LTP (Townsend et al., 2006a). In addition, DHK has a half maximal inhibitory constant (IC₅₀) of 23 μ M, indicating that 100 μ M will inhibit a large proportion of GLT-1. These data indicate that even when the majority of GLT-1 is inhibited, the other transporters can make significant contributions to clearance of glutamate (Pinky et al., 2018) and prevent any LTP impairment from occurring. Therefore, in contrast to the conclusions drawn from prior studies (Li et al., 2009, 2011; Varga et al., 2015; Lei et al., 2016), our results suggest that it is unlikely that the degree of GLT-1 dysfunction observed in disease states is sufficient to cause a plasticity deficit.

Interestingly, the IC₅₀ of TBOA for GLT-1 is 6 μ M indicating that the majority of GLT-1 is also inhibited with 15 μ M TBOA. The IC₅₀ for GLAST and EAAC1 is 70 μ M and 6 μ M, respectively. Therefore, while GLAST is largely unaffected by 15 μ M TBOA, the majority of EAAC1 transporters are likely impaired. EAAC1 has been shown to act as a buffer of extracellular glutamate (Scimemi et al., 2009), and is often regarded as being less important for the clearance of glutamate and more important for its ability to transport cysteine (Peghini et al., 1997; Aoyama et al., 2006; Vandenberg and Ryan, 2013). Since the major difference between using 100 μ M DHK and 15 μ M TBOA is the ability of TBOA to block EAAC1, it is possible that this transporter has previously been underestimated and functioning is vital for facilitating LTP. Another possibility for this difference may be the sheer magnitude of glutamate transporters blocked. 100 μ M DHK causes a two-fold increase in extracellular glutamate while 15 μ M TBOA causes a three fold increase in extracellular glutamate, it may just be that the magnitude of deficit reached by inhibiting EAAC1 and GLT-1 is required to impair plasticity. EAAC1 is difficult to study due to the lack of EAAC1-selective inhibitors. More studies will need to be conducted to determine whether EAAC1 has a role in the LTP impairments observed when glutamate uptake is compromised.

4.2 Mechanism of TBOA-mediated LTP impairment

Overactivation of extrasynaptic and/or GluN2B-containing NMDARs have recently been shown to prevent LTP and even induce LTD (Liu et al., 2004; Li et al., 2009, 2011; Brigman et al., 2010; Mucke and Selkoe, 2012; Paoletti et al., 2013; Varga et

al., 2015). To our surprise, the GluN2B-containing antagonist, ifenprodil, did not restore the LTP deficit due to TBOA in our model. ERK is essential for LTP induced by TBS and is differentially regulated via NMDAR activation; synaptic NMDARs activate ERK (Xu et al., 2009; Wang et al., 2013; Zhu et al., 2015) while extrasynaptic or GluN2B-containing NMDARs inhibit ERK (Myung et al., 2005; Ivanov et al., 2006). We showed that pERK is actually enhanced post-LTP induction in the presence of TBOA, further providing evidence that our experimental conditions do not enhance GluN2B-containing or extrasynaptic NMDAR activity. We also showed that inhibition of GSK3, a kinase involved in the LTD (Morfini et al., 2004; Lee et al., 2005; Szatmari et al., 2005; Peineau et al., 2007, 2008), does not prevent the TBOA-mediated LTP impairment. In all, these data indicate that the TBOA-mediated LTP impairment is not due to enhanced extrasynaptic or GluN2B-containing NMDAR activity.

Surprisingly, while LTP was normal in the presence of the GSK inhibitor alone, there was a robust LTD in the presence of the GSK inhibitor and TBOA, this suggests that the role of GSK3 in plasticity is more complex than we first thought. In support of this rationale, GSK3 can prevent excitotoxicity due to amyloid beta application by internalizing NMDARs (Deng et al., 2014). Since we observed a reduction in the fEPSP area due to NMDAR desensitization during TBS, it is possible that TBOA caused a reduction in NMDAR-mediated current through a mechanism involving GSK3 activity. However, more research will be required to determine whether there is a causal link between NMDAR-mediated current and GSK3 in the presence of TBOA.

Since TBOA promoted excess extracellular glutamate accumulation during TBS, we thought it was possible that overaction of NMDARs in general was impairing LTP in our model. However, as observed, a low concentration of the NMDAR-antagonist D APV did not prevent the LTP deficit. In addition, when we look at the AUC of the fEPSP during TBS, we observed a surprising decrease in the NMDAR-mediated current due to TBOA. These data suggest that there was no pathological overaction of NMDAR activity occur in our model.

In addition, we confirmed that the TBOA-mediated LTP impairment was not due to NMDAR-independent activity since we did not observe a robust LTD in the presence of the NMDAR antagonists, MK-801 and D-APV. Recent evidence has suggested that NMDARs can have metabotropic activity (Nabavi et al., 2013a, 2013b; Dore et al., 2017). These studies show that when the pore of the NMDAR is blocked by MK-801, TBS induced a robust LTD suggesting that ion influx is not required for LTD. Here we tested MK-801 to determine whether our LTP impairment was due to metabotropic NMDAR activity. However, we found no potentiation or depression in the presence of MK-801 with or without TBOA application indicating that metabotropic NMDAR activity was not occurring in our experimental design.

The lack of mGluR involvement was also suggested by our MK-801, D-APV and mGluR 1 antagonist, AIDA experiments (Huber and Luscher, 2010). This was supported by our paired-pulse ratio experiments. Presynaptic LTD, as measured by paired pulse ratio, is dependent on mGluR activation (Watabe et al., 2002). The paired pulse ratio did not change in the presence of TBOA and AIDA did not prevent the TBOA-mediated LTP

impairment. In all, these data suggest that in the presence of TBOA, mGluRs are not activated to impair synaptic plasticity.

Calcium influx initiates intracellular signalling cascades which strengthens the synaptic connection (Bliss and Collingridge, 1993; Malenka and Bear, 2004; Kauer and Malenka, 2007). Surprisingly, despite the reduction in NMDAR-mediated current and lack of increased activation of any other glutamate receptors, we observed a robust increase in intracellular calcium in the presence of TBOA as compared to controls (Fig 15). Of interest were calcium permeable AMPARs, calcium release via intracellular stores, and L-VGCCs. Preventing release or influx through any of these mechanisms significantly reduced the intracellular calcium due to TBOA; however, only blocking L-VGCCs restored the LTP deficit in the presence of TBOA. L-VGCCs are not required for protein-synthesis independent forms of LTP such as the one we use in this experimental design (Raymond, 2007). It is unknown how this excess calcium influx through NMDARs occurs. It is possible that there is an increase in the number of channels in the postsynaptic neuron or already present L-VGCCs are phosphorylated to alter their open probability or increase conductance (Thibault and Landfield, 1996; Davare and Hell, 2003; Folci et al., 2018). The increase in calcium influx may also be attributed to glutamate spillover induced by TBOA resulting in larger postsynaptic depolarizations within the micro-environment of the L-VGCCs. TBOA, but not DHK, resulted in increased ambient glutamate levels. The increased ambient glutamate can slightly depolarize neurons and bring them closer to the threshold of L-VGCCs. The precise

mechanism by which the increase in intracellular calcium occurs can be considered in future studies.

Calpains have recently been dubbed the ‘yin and yang of synaptic plasticity’ for their opposing effects on synaptic plasticity (Baudry and Bi, 2016). Calpain-1 facilitates the induction of TBS-LTP while calpain-2 limits the amount of potentiation that can occur post-induction (Wang et al., 2014; Baudry et al., 2015; Zhu et al., 2015; Baudry and Bi, 2016). Calpain-2 can be activated by millimolar concentrations of calcium (Baudry and Bi, 2016) and pERK (Glading et al., 2004; Chen et al., 2010). In the presence of TBOA, TBS resulted in excessive cytosolic calcium and pERK hyperactivation, leading us to hypothesize that calpain-2 may be recruited under these conditions. As expected, preventing calpain activity post-LTP induction prevented the TBOA-mediated LTP impairment. In our experimental design, we did not determine whether calpain activity was increased due to pERK activity, increased intracellular calcium, or both—this can be determined in future studies. It is important to note that in the original study on calpain activity post LTP induction there was an increase in the magnitude of LTP after inhibiting calpain activity 10 minutes post-induction (Wang et al., 2014). However, we observed a slight but non-significant decrease in the magnitude of potentiation with the inhibitor alone. This discrepancy is likely due to subtle differences in our methodologies—in the original study Sprague Dawley rats were used and fEPSPs were recorded at 33 °C while we used C57BL/6 mice and recorded fEPSPs at 24 °C. The species and/or temperature differences likely alter the time course of calpain-1 and calpain-2 slightly causing the magnitude of our potentiation to be reduced as compared to Wang and colleagues (2014).

4.3 Relevance to Neurodegenerative Disease

As mentioned, many studies demonstrate a 13-30% deficit in glutamate clearance in animal models of neurodegenerative disease; such a deficit is believed to be responsible for the LTP impairment observed (Li et al., 2009, 2011; Varga et al., 2015; Lei et al., 2016). We show that even with a two-fold deficit in clearance due to 100 μ M DHK, no deficit in the magnitude of potentiation is observed. While it is unlikely that deficits in clearance required to impair synaptic plasticity are ever reached in disease states, it is possible that other components of the mechanism of impairment occur in AD. For example, pERK has been found to be increased in animal models of AD (Feld et al., 2014). In addition, a calcium hypothesis of AD postulates that abnormal calcium signalling underlies AD pathology (Samad et al., 2017; Ahmad et al., 2018). L-VGCC expression and conductance are normally increased during aging (Thibault and Landfield, 1996; Davare and Hell, 2003); however, their expression and conductance is increased further in animal models of AD (Anekonda et al., 2011; Kim and Rhim, 2011; Wang and Mattson, 2014). Therefore, it is possible that pathological increases in intracellular calcium contribute to the LTP impairments observed in neurodegenerative disease. For our study, we used young adult mice. Future studies will assess whether a TBOA-mediated LTP impairment is observed in older mice and whether LTP at this age is more sensitive to impaired glutamate clearance. We hypothesize that at older ages, when there is an increase in calcium influx through L-VGCCs, there will likely be an LTP impairment with lower concentrations of TBOA. Increased calpain activity has been observed in

humans and models of neurodegenerative diseases (Tsuji et al., 1998; Gafni and Ellerby, 2002; Gladding et al., 2012; Ahmad et al., 2018). Therefore, this increased calpain activity in combination with increased L-VGCC activity, may very well impair LTP in models of AD.

4.4 Conclusion

To our knowledge, we are the first to characterize the relationship between glutamate clearance and synaptic plasticity in real-time and *in situ*. Three-fold increases in extracellular glutamate are required to impair synaptic plasticity. Our results suggest that subtle reductions in GLT-1, the most abundant transporter, are unlikely to have a significant impact on the magnitude of potentiation. In addition, more studies should be conducted on the role of EAAC1 and whether this significantly contributes to the regulation of extracellular glutamate during plasticity inducing stimuli. We found that the LTP impairment due to slow glutamate clearance is not caused by excessive activation of extrasynaptic or GluN2B-containing NMDARs, as previously suggested. Instead, increased activity of pERK and/or calcium influx through L-VGCCs cause an increase in calpain activity to impair synaptic plasticity. While it is unlikely that these deficits will ever be reached in disease states, it is expected that components of this mechanism will occur through excess activation of pERK, L-type VGCCs, and/or calpain activity.

References

- Ahmad F, Das D, Kommaddi RP, Diwakar L, Gowaikar R, Rupanagudi KV, Bennett DA, Ravindranath V (2018) Isoform-specific hyperactivation of calpain-2 occurs presymptomatically at the synapse in Alzheimer's disease mice and correlates with memory deficits in human subjects. *Sci Rep* 8:13119.
- Al-Hallaq RA, Conrads TP, Veenstra TD, Wenthold RJ (2007) NMDA di-heteromeric receptor populations and associated proteins in rat hippocampus. *J Neurosci* 27:8334–8343.
- Anekonda TS, Quinn JF, Harris C, Frahler K, Wadsworth TL, Woltjer RL (2011) L-type voltage-gated calcium channel blockade with isradipine as a therapeutic strategy for Alzheimer's disease. *Neurobiol Dis* 41:62–70.
- Aoyama K, Sang WS, Hamby AM, Liu J, Wai YC, Chen Y, Swanson RA (2006) Neuronal glutathione deficiency and age-dependent neurodegeneration in the EAAC1 deficient mouse. *Nat Neurosci* 9:119–126.
- Bains JS, Cusulin JIW, Inoue W (2015) Stress-related synaptic plasticity in the hypothalamus. *Nat Rev Neurosci* 16:377–388.
- Baudry M, Bi X (2016) Calpain-1 and calpain-2: The yin and yang of synaptic plasticity and neurodegeneration. *Trends Neurosci* 39:235–245.
- Baudry M, Zhu G, Liu Y, Wang Y, Briz V, Bi X (2015) Multiple cellular cascades participate in long-term potentiation and in hippocampus-dependent learning. *Brain Res* 1621:73–81.
- Bergles DE, Dzubay J, Jahr C (1997) Glutamate transporter currents in Bergmann glial cells follow the time course of extrasynaptic glutamate. *Proc Natl Acad Sci U S A* 94:14821–

14825.

Bergles DE, Jahr CE (1997) Synaptic activation of glutamate transporters in hippocampal astrocytes. *Neuron* 19:1297–1308.

Bliss TVP, Collingridge GL (1993) A synaptic model of memory: Long-term potentiation in the hippocampus. *Nature* 361:31–39.

Bliss TVP, Collingridge GL, Kaang BK, Zhuo M (2016) Synaptic plasticity in the anterior cingulate cortex in acute and chronic pain. *Nat Rev Neurosci* 17:485–496.

Bliss TVP, Lomo T (1973) Long-lasting potentiation of synaptic transmission in the dentate area of the anaesthetized rabbit following stimulation of the perforant path. *J Physiol* 232:331–356.

Bonde C, Sarup A, Schousboe A, Gegelashvili G, Zimmer J, Noraberg J (2003) Neurotoxic and neuroprotective effects of the glutamate transporter inhibitor DL-threo-beta-benzyloxyaspartate (DL-TBOA) during physiological and ischemia-like conditions. *Neurochem Int* 43:371–380.

Bosch M, Castro J, Saneyoshi T, Matsuno H, Sur M, Hayashi Y (2014) Structural and molecular remodeling of dendritic spine substructures during long-term potentiation. *Neuron* 82:444–459 Available at: <http://dx.doi.org/10.1016/j.neuron.2014.03.021>.

Bradley CA, Peineau S, Taghibiglou C, Nicolas CS, Whitcomb DJ, Bortolotto ZA, Kaang B-K, Cho K, Wang YT, Collingridge GL (2012) A pivotal role of GSK-3 in synaptic plasticity. *Front Mol Neurosci* 5:13 Available at: <http://www.ncbi.nlm.nih.gov/pmc/articles/PMC3279748/>.

- Brigman JL, Wright T, Talani G, Prasad-Mulcare S, Jinde S, Seabold GK, Mathur P, Davis MI, Bock R, Gustin RM, Colbran RJ, Alvarez VA, Nakazawa K, Delpire E, Lovinger DM, Holmes A (2010) Loss of GluN2B-containing NMDA receptors in CA1 hippocampus and cortex impairs long-term depression, reduces dendritic spine density, and disrupts learning. *J Neurosci* 30:4590–4600.
- Carulla P, Llorens F, Matamoros-Angles A, Aguilar-Calvo P, Espinosa JC, Gavín R, Ferrer I, Legname G, Torres JM, Del Río JA (2015) Involvement of PrP C in kainate-induced excitotoxicity in several mouse strains. *Sci Rep* 5:1–15 Available at: <http://dx.doi.org/10.1038/srep11971>.
- Chen H, Libertini SJ, Wang Y, Kung HJ, Ghosh P, Mudryj M (2010) ERK regulates calpain 2-induced androgen receptor proteolysis in CWR22 relapsed prostate tumor cell lines. *J Biol Chem* 285:2368–2374.
- Connor SA, Wang YT (2016) A Place at the Table: LTD as a Mediator of Memory Genesis. *Neuroscientist* 22:359–371.
- Cummings JA, Mulkey RM, Nicoll RA, Malenka RC (1996) Ca²⁺ signaling requirements for long-term depression in the hippocampus. *Neuron* 16:825–833.
- Currie DN, Kelly JS (1981) Glial versus neuronal uptake of glutamate. *J Exp Biol* 95:181–193.
- Danbolt NC (2001) Glutamate uptake. *Prog Neurobiol* 65:1–105.
- Danbolt NC, Furness DN, Zhou Y (2016) Neuronal vs glial glutamate uptake: Resolving the conundrum. *Neurochem Int* 98:29–45.
- Davare MA, Hell JW (2003) Increased phosphorylation of the neuronal L-type Ca²⁺ channel

- Cav1.2 during aging. *Proc Natl Acad Sci* 100:16018–16023 Available at:
<http://www.pnas.org/cgi/doi/10.1073/pnas.2236970100>.
- Deng Y, Xiong Z, Chen P, Wei J, Chen S, Yan Z (2014) Beta-amyloid impairs the regulation of N-methyl-D-aspartate receptors by glycogen synthase kinase 3. *Neurobiol Aging* 35:449–459.
- Diamond JS, Jahr CE (1997) Transporters buffer synaptically released glutamate on a submillisecond time scale. *J Neurosci* 17:4672–4687.
- Dodd PR, Hardy JA, Oakley AE, Edwardson JA, Perry EK, Delaunoy JP (1981) A rapid method for preparing synaptosomes: Comparison, with alternative procedures. *Brain Res* 226:107–118.
- Dore K, Aow J, Malinow R (2016) The emergence of NMDA receptor metabotropic function: Insights from imaging. *Front Synaptic Neurosci* 8:1–9.
- Dore K, Stein IS, Brock JA, Castillo PE, Zito K, Sjöström PJ (2017) Unconventional NMDA Receptor Signaling. *J Neurosci* 37:10800–10807.
- Drejer J, Larsson OM, Schousboe A (1982) Characterization of L-glutamate uptake into and release from astrocytes and neurons cultured from different brain regions. *Exp Brain Res* 47:259–269.
- Erreger K, Dravid SM, Banke TG, Wyllie DJA, Traynelis SF (2005) Subunit-specific gating controls rat NR1/NR2A and NR1/NR2B NMDA channel kinetics and synaptic signalling profiles. *J Physiol* 563:345–358.
- Faideau M, Kim J, Cormier K, Gilmore R, Welch M, Auregan G, Dufour N, Guillermier M,

- Brouillet E, Hantraye P, Déglon N, Ferrante RJ, Bonvento G (2010) In vivo expression of polyglutamine-expanded huntingtin by mouse striatal astrocytes impairs glutamate transport: a correlation with Huntington's disease subjects. *Hum Mol Genet* 19:3053–3067.
- Feld M, Krawczyk MC, Sol Fustinana M, Blake MG, Baratti CM, Romano A, Boccia MM (2014) Decrease of ERK/MAPK overactivation in prefrontal cortex reverses early memory deficit in a mouse model of Alzheimer's disease. *J Alzheimers Dis* 40:69–82.
- Folci A, Steinberger A, Lee B, Stanika R, Scheruebel S, Campiglio M, Ramprecht C, Pelzmann B, Hell JW, Obermair GJ, Heine M, Di Biase V (2018) Molecular mimicking of C-terminal phosphorylation tunes the surface dynamics of CaV1.2 calcium channels in hippocampal neurons. *J Biol Chem* 293:1040–1053.
- Gafni J, Ellerby LM (2002) Calpain activation in Huntington's disease. *J Neurosci* 22:4842–4849.
- Giovannini MG (2006) The role of the extracellular signal-regulated kinase pathway in memory encoding. *Rev Neurosci* 17:619–634.
- Gladding CM, Sepers MD, Xu J, Zhang LYJ, Milnerwood AJ, Lombroso PJ, Raymond LA (2012) Calpain and striatal-enriched protein tyrosine phosphatase (STEP) activation contribute to extrasynaptic NMDA receptor localization in a Huntington's disease mouse model. *Hum Mol Genet* 21:3739–3752.
- Glading A, Bodnar RJ, Reynolds IJ, Shiraha H, Satish L, Potter DA, Blair HC, Wells A (2004) Epidermal growth factor activates m-calpain (calpain II), at least in part, by extracellular signal-regulated kinase-mediated phosphorylation. *Mol Cell Biol* 24:2499–2512.

- Groc L, Heine M, Cousins SL, Stephenson FA, Lounis B, Cognet L, Choquet D (2006) NMDA receptor surface mobility depends on NR2A-2B subunits. *Proc Natl Acad Sci* 103.
- Hardingham GE, Bading H (2010) Synaptic versus extrasynaptic NMDA receptor signalling: implications for neurodegenerative disorders. *Nat Rev Neurosci* 11:682–696.
- Harris AZ, Pettit DL (2007) Extrasynaptic and synaptic NMDA receptors form stable and uniform pools in rat hippocampal slices. *J Neurosci* 27:509–519.
- Haugeto O, Ullensvang K, Levy LM, Chaudhry FA, Honore T, Nielsen M, Lehre KP, Danbolt NC (1996) Brain glutamate transporter proteins form homomultimers. *J Biol Chem* 271:27715–27722.
- Hell JW (2016) How Ca²⁺-permeable AMPA receptors, the kinase PKA, and the phosphatase PP2B are intertwined in synaptic LTP and LTD. *Sci Signal* 9:1–5.
- Holmseth S, Dehnes Y, Huang YH, Follin-Arbelet V, Grutle NJ, Mylonakou MN, Plachez C, Zhou Y, Furness DN, Bergles DE, Lehre KP, Danbolt NC (2012) The density of EAAC1 (EAAT3) glutamate transporters expressed by neurons in the mammalian CNS. *J Neurosci* 32:6000–6013.
- Huber KM, Luscher C (2010) Group 1 mGluR-dependent synaptic long-term depression (mGluR-LTD): mechanisms and implications for circuitry & disease. *Neuron* 65:445–459.
- Huganir RL, Nicoll RA (2013) AMPARs and synaptic plasticity: The last 25 years. *Neuron* 80:704–717.
- Ivanov A, Pellegrino C, Rama S, Dumalska I, Salyha Y, Ben-Ari Y, Medina I (2006) Opposing role of synaptic and extrasynaptic NMDA receptors in regulation of the extracellular signal-

regulated kinases (ERK) activity in cultured rat hippocampal neurons. *J Physiol* 572:789–798.

Jo J, Whitcomb DJ, Olsen KM, Kerrigan TL, Lo S-C, Bru-Mercier G, Dickinson B, Scullion S, Sheng M, Collingridge G, Cho K (2011) A β 1–42 inhibition of LTP is mediated by a signaling pathway involving caspase-3, Akt1 and GSK-3 β . *Nat Neurosci* 14:545–547
Available at: <http://www.nature.com/doi/10.1038/nn.2785>.

Kanai Y, Hediger MA (1992) Primary structure and functional characterization of a high-affinity glutamate transporter. *Nature* 360:467–471.

Katagiri H, Tanaka K, Manabe T (2001) Requirement of appropriate glutamate concentrations in the synaptic cleft for hippocampal LTP induction. *Eur J Neurosci* 14:547–553.

Kauer JA, Malenka RC (2007) Synaptic plasticity and addiction. *Nat Rev Neurosci* 8:844.

Kellermayer B, Ferreira JS, Dupuis J, Levet F, Grillo-Bosch D, Bard L, Linarès-Loyez J, Bouchet D, Choquet D, Rusakov DA, Bon P, Sibarita JB, Cognet L, Sainlos M, Carvalho AL, Groc L (2018) Differential Nanoscale Topography and Functional Role of GluN2-NMDA Receptor Subtypes at Glutamatergic Synapses. *Neuron* 100:106–119.e7.

Kessels HW, Malinow R (2009) Synaptic AMPA receptor plasticity and behavior. *Neuron* 61:340–350.

Kessels HW, Nabavi S, Malinow R (2013) Metabotropic NMDA receptor function is required for beta-amyloid-induced synaptic depression. *Proc Natl Acad Sci* 110:4033–4038.

Kim S, Rhim H (2011) Effects of amyloid-beta peptides on voltage-gated L-type Ca(V)1.2 and Ca(V)1.3 Ca(2+) channels. *Mol Cells* 32:289–294.

- Koeglsperger T, Li S, Brenneis C, Saulnier JL, Mayo L, Carrier Y, Selkoe DJ, Weiner HL (2013) Impaired glutamate recycling and GluN2B-mediated neuronal calcium overload in mice lacking TGF- β 1 in the CNS. *Glia* 40:1301–1315.
- Kumar A, Foster TC (2014) Interaction of DHPG-LTD and synaptic-LTD at senescent CA3-CA1 hippocampal synapses. *Hippocampus* 24:466–475.
- Larson J, Lynch G (1988) Role of N-methyl-D-aspartate receptors in the induction of synaptic potentiation by burst stimulation patterned after the hippocampal θ -rhythm. *Brain Res* 441:111–118.
- Le Meur K, Galante M, Angulo MC, Audinat E (2007) Tonic activation of NMDA receptors by ambient glutamate of non-synaptic origin in the rat hippocampus. *J Physiol* 580:373–383.
- Lee Y-I, Seo M, Kim Y, Kim S-Y, Kang UG, Kim Y-S, Juhn Y-S (2005) Membrane depolarization induces the undulating phosphorylation/dephosphorylation of glycogen synthase kinase 3 β , and this dephosphorylation involves protein phosphatases 2A and 2B in SH-SY5Y human neuroblastoma cells. *J Biol Chem* 280:22044–22052.
- Lei M, Xu H, Li Z, Wang Z, O'Malley TT, Zhang D, Walsh DM, Xu P, Selkoe DJ, Li S (2016) Soluble A β oligomers impair hippocampal LTP by disrupting glutamatergic/GABAergic balance. *Neurobiol Dis* 85:111–121.
- Levy LM, Lehre KP, Rolstad B, Danbolt NC (1993) A monoclonal antibody raised against an [Na⁺K⁺]-coupled l-glutamate transporter purified from rat brain confirms glial cell localization. *FEBS Lett* 317:79–84.
- Li S, Hong S, Shepardson NE, Walsh DM, Shankar GM, Selkoe D (2009) Soluble oligomers of

amyloid β -protein facilitate hippocampal long-term depression by disrupting neuronal glutamate uptake. *Neuron* 62:788–801.

Li S, Jin M, Koeglsperger T, Shepardson NE, Shankar GM, Selkoe DJ (2011) Soluble Abeta oligomers inhibit long-term potentiation through a mechanism involving excessive activation of extrasynaptic NR2B-containing NMDA receptors. *J Neurosci* 31:6627–6638.

Liévens JC, Woodman B, Mahal A, Spasic-Boscovic O, Samuel D, Kerkerian-Le Goff L, Bates GP (2001) Impaired glutamate uptake in the R6 Huntington's disease transgenic mice. *Neurobiol Dis* 8:807–821.

Lisman J (1994) The CaM kinase II hypothesis for the storage of synaptic memory. *Trends Neurosci* 17:406–412.

Liu D dan, Yang Q, Li S tian (2013) Activation of extrasynaptic NMDA receptors induces LTD in rat hippocampal CA1 neurons. *Brain Res Bull* 93:10–16.

Liu LD, Wong TP, Pozza MF, Lingenhoehl K, Wang YS, Sheng M, Auberson YP, Wang YT (2004) Role of NMDA receptor subtypes in governing the direction of hippocampal synaptic plasticity. *Science* (80-) 304:1021–1024.

Liu M-G, Li H-S, Li W-G, Wu Y-J, Deng S-N, Huang C, Maximyuk O, Sukach V, Krishtal O, Zhu MX, Xu T-L (2016a) Acid-sensing ion channel 1a contributes to hippocampal LTP inducibility through multiple mechanisms. *Sci Rep* 6:23350 Available at: <http://www.nature.com/articles/srep23350>.

Liu Y, Wang Y, Zhu G, Sun J, Bi X, Baudry M (2016b) A calpain-2 selective inhibitor enhances learning & memory by prolonging ERK activation. *Neuropharmacology* 105:471–477.

- Lu WY, Man HY, Ju W, Trimble WS, MacDonald JF, Wang YT (2001) Activation of synaptic NMDA receptors induces membrane insertion of new AMPA receptors and LTP in cultured hippocampal neurons. *Neuron* 29:243–254.
- Malenka RC, Bear MF (2004) LTP and LTD: An embarrassment of riches. *Neuron* 44:5–21.
- Marvin JS, Borghuis BG, Tian L, Cichon J, Harnett MT, Akerboom J, Gordus A, Renninger SL, Chen T-W, Bargmann CI, Orger MB, Schreiter ER, Demb JB, Gan W-B, Hires SA, Looger LL (2013) An optimized fluorescent probe for visualizing glutamate neurotransmission. *Nat Methods* 10:162–170.
- Matsugami TR, Tanemura K, Mieda M, Nakatomi R, Yamada K, Kondo T, Ogawa M, Obata K, Watanabe M, Hashikawa T, Tanaka K (2006) Indispensability of the glutamate transporters GLAST and GLT1 to brain development. *Proc Natl Acad Sci* 103:12161–12166.
- Miller BR, Dorner JL, Shou M, Sari Y, Barton SJ, Sengelaub DR, Kennedy RT, Rebec G V (2008) Up-regulation of GLT1 expression increases glutamate uptake and attenuates the Huntington's disease phenotype in the R6/2 mouse. *Neuroscience* 153:329–337.
- Mookherjee P, Green PS, Watson GS, Marques MA, Tanaka K, Meeker KD, Meabon JS, Li N, Zhu P, Olson VG, Cook DG (2011) GLT-1 loss accelerates cognitive deficit onset in an Alzheimer's disease animal model. *J Alzheimers Dis* 26:447–455.
- Morfini G, Szebenyi G, Brown H, Pant HC, Pignino G, DeBoer S, Beffert U, Brady ST (2004) A novel CDK5-dependent pathway for regulating GSK3 activity and kinesin-driven motility in neurons. *EMBO J* 23:2235–2245.
- Mucke L, Selkoe DJ (2012) Neurotoxicity of amyloid b protein. :1–18.

- Mulkey RM, Endo S, Shenolikar S, Malenka RC (1994) Involvement of a calcineurin/ inhibitor-1 phosphatase cascade in hippocampal long-term depression. *Nature* 369:486.
- Myung JK, Dunah AW, Yu TW, Sheng M (2005) Differential roles of NR2A- and NR2B-containing NMDA receptors in Ras-ERK signaling and AMPA receptor trafficking. *Neuron* 46:745–760.
- Nabavi S, Fox R, Alfonso S, Aow J, Malinow R (2013a) GluA1 trafficking and metabotropic NMDA: addressing results from other laboratories inconsistent with ours. *Philos Trans R Soc B Biol Sci* 369:1–3.
- Nabavi S, Kessels HW, Alfonso S, Aow J, Fox R, Malinow R (2013b) Metabotropic NMDA receptor function is required for NMDA receptor-dependent long-term depression. *Proc Natl Acad Sci* 110:4027–4032.
- Nakahata Y, Yasuda R (2018) Plasticity of spine structure: local signaling, translation and cytoskeletal reorganization. *Front Synaptic Neurosci* 10:29.
- Nowak L, Bregestovski P, Ascher P, Herbet A, Prochiantz A (1984) Magnesium gates glutamate-activated channels in mouse central neurones. *Nature* 307:462–465.
- Opazo P, Sainlos M, Choquet D (2012) Regulation of AMPA receptor surface diffusion by PSD-95 slots. *Curr Opin Neurobiol* 22:453–460.
- Otis MP, Kavanaugh TS (2000) Isolation of current components and partial reaction cycles in the glial glutamate transporter EAAT2. *J Neurosci* 20:2749–2757.
- Otto T, Eichenbaum H, Wible CG, Wiener SI (1991) Learning-related patterns of CA1 spike trains parallel stimulation parameters optimal for inducing hippocampal long-term

- potentiation. *Hippocampus* 1:181–192.
- Paoletti P, Bellone C, Zhou Q (2013) NMDA receptor subunit diversity: Impact on receptor properties, synaptic plasticity and disease. *Nat Rev Neurosci* 14:383–400.
- Papouin T, Ladépêche L, Ruel J, Sacchi S, Labasque M, Hanini M, Groc L, Pollegioni L, Mothet J-P, Oliet SHR (2012) Synaptic and extrasynaptic NMDA receptors are gated by different endogenous coagonists. *Cell* 150:633–646.
- Parsons MP, Kang R, Buren C, Dau A, Southwell AL, Doty CN, Sanders SS, Hayden MR, Raymond LA (2014) Bidirectional control of Postsynaptic Density-95 (PSD-95) clustering by Huntingtin. *J Biol Chem* 289:3518–3528.
- Parsons MP, Vanni MP, Woodard CL, Kang R, Murphy TH, Raymond LA (2016) Real-time imaging of glutamate clearance reveals normal striatal uptake in Huntington disease mouse models. *Nat Commun* 7:11251.
- Peghini P, Janzen J, Stoffel W (1997) Glutamate transporter EAAC-1-deficient mice develop dicarboxylic aminoaciduria and behavioral abnormalities but no neurodegeneration. *EMBO J* 16:3822–3832.
- Peineau S, Bradley C, Taghibiglou C, Doherty A, Bortolotto ZA, Wang YT, Collingridge GL (2008) The role of GSK-3 in synaptic plasticity. *Br J Pharmacol* 153 Suppl:S428-37.
- Peineau S, Taghibiglou C, Bradley C, Wong TP, Liu L, Lu J, Lo E, Wu D, Saule E, Bouschet T, Matthews P, Isaac JTR, Bortolotto ZA, Wang YT, Collingridge GL (2007) LTP inhibits LTD in the hippocampus via regulation of GSK3 β . *Neuron* 53:703–717.
- Perea G, Navarrete M, Araque A (2009) Tripartite synapses: astrocytes process and control

synaptic information. *Trends Neurosci* 32:421–431.

Petr GT, Schultheis LA, Hussey KC, Sun Y, Dubinsky JM, Aoki C, Rosenberg PA (2013)

Decreased expression of GLT-1 in the R6/2 model of Huntington's disease does not worsen disease progression. *Eur J Neurosci* 38:2477–2490.

Petr GT, Sun Y, Frederick NM, Zhou Y, Dhamne SC, Hameed MQ, Miranda C, Bedoya EA,

Fischer KD, Armsen W, Wang J, Danbolt NC, Rotenberg A, Aoki CJ, Rosenberg PA

(2015) Conditional deletion of the glutamate transporter GLT-1 reveals that astrocytic GLT-1 protects against fatal epilepsy while neuronal GLT-1 contributes significantly to glutamate uptake into synaptosomes. *J Neurosci* 35:5187–5201.

Petralia RS, Wang YX, Hua F, Yi Z, Zhou A, Ge L, Stephenson FA, Wenthold RJ (2010)

Organization of NMDA receptors at extrasynaptic locations. *Neuroscience* 167:68–87.

Pickard L, Noel J, Duckworth JK, Fitzjohn SM, Henley JM, Collingridge GL, Molnar E (2001)

Transient synaptic activation of NMDA receptors leads to the insertion of native AMPA receptors at hippocampal neuronal plasma membranes. *Neuropharmacology* 41:700–713.

Pinky NF, Wilkie CM, Barnes JR, Parsons MP (2018) Region- and activity-dependent regulation

of extracellular glutamate. *J Neurosci* 38:5351–5366.

Piskorowski RA, Chevaleyre V (2012) Synaptic integration by different dendritic compartments

of hippocampal CA1 and CA2 pyramidal neurons. *Cell Mol Life Sci* 69:75–88.

Raiteri L, Raiteri M (2000) Synaptosomes still viable after 25 years of superfusion. *Neurochem*

Res 25:1265–1274.

Raymond CR (2007) LTP forms 1, 2 and 3: Different mechanisms for the 'long' in long-term

potentiation. *Trends Neurosci* 30:167–175.

Rothstein JD, Martin L, Levey AI, Dykes-Hoberg M, Jin L, Wu D, Nash N, Kuncl RW (1994)

Localization of neuronal and glial glutamate transporters. *Neuron* 13:713–725.

Sakimura K, Kutsuwada T, Ito I, Manabe T, Takayama C, Kushiya E, Yagi T, Aizawa S, Inoue

Y, Sugiyama H, Mishina M (1995) Reduced hippocampal LTP and spatial learning in mice lacking NMDA receptor $\epsilon 1$ subunit. *Nature* 373:151.

Samad N, Ishaq S, Bano S, Manzoor N (2017) Calcium regulation in Alzheimer's disease:

Mechanistic understanding. *J Coll Physicians Surg Pak* 27:566–571.

Scimemi A, Meabon JS, Woltjer RL, Sullivan JM, Diamond JS, Cook DG (2013) Amyloid- $\beta 1$ -

42 slows clearance of synaptically released glutamate by mislocalizing astrocytic GLT-1.

Ann Intern Med 158:5312–5318.

Scimemi A, Tian H, Diamond JS (2009) Neuronal transporters regulate glutamate clearance,

NMDA receptor activation, and synaptic plasticity in the hippocampus. *J Neurosci*

29:14581–14595.

Selkoe DJ, Hardy J (2016) The amyloid hypothesis of Alzheimer's disease at 25 years. *EMBO*

Mol Med 8:595–608 Available at:

<http://embomolmed.embopress.org/lookup/doi/10.15252/emmm.201606210>.

Shouval HZ, Bear MF, Cooper LN (2002) A unified model of NMDA receptor-dependent

bidirectional synaptic plasticity. *Proc Natl Acad Sci U S A* 99:10831–10836.

Soni N, Reddy BVK, Kumar P (2014) GLT-1 transporter: An effective pharmacological target

for various neurological disorders. *Pharmacol Biochem Behav* 127:70–81.

- Steigerwald F, Schulz TW, Schenker LT, Kennedy MB, Seeburg PH, Kohr G (2000) C-Terminal truncation of NR2A subunits impairs synaptic but not extrasynaptic localization of NMDA receptors. *J Neurosci* 20:4573–4581.
- Sweatt JD (2004) Mitogen-activated protein kinases in synaptic plasticity and memory. *Curr Opin Neurobiol* 14:311–317.
- Szatmari E, Habas A, Yang P, Zheng J-J, Hagg T, Hetman M (2005) A positive feedback loop between glycogen synthase kinase 3beta and protein phosphatase 1 after stimulation of NR2B NMDA receptors in forebrain neurons. *J Biol Chem* 280:37526–37535.
- Tanaka K, Watase K, Manabe T, Yamada K, Watanabe M, Takahashi K, Iwama H, Nishikawa T, Ichihara N, Kikuchi T, Okuyama S, Kawashima N, Hori S, Takimoto M, Wada K (1997) Epilepsy and exacerbation of brain injury in mice lacking the glutamate transporter GLT-1. *Science* (80-) 276:1699–1703.
- Thibault O, Landfield PW (1996) Increase in single L-type calcium channels in hippocampal neurons during aging. *Science* 272:1017–1020.
- Townsend M, Shankar GM, Mehta T, Walsh DM, Selkoe DJ (2006a) Effects of secreted oligomers of amyloid β -protein on hippocampal synaptic plasticity: a potent role for trimers. *J Physiol* 572:477–492.
- Townsend M, Shankar GM, Mehta T, Walsh DM, Selkoe DJ (2006b) Effects of secreted oligomers of amyloid β -protein on hippocampal synaptic plasticity: A potent role for trimers. *J Physiol* 572:477–492.
- Tsuji T, Shimohama S, Kimura J, Shimizu K (1998) m-Calpain (calcium-activated neutral

- proteinase) in Alzheimer's disease brains. *Neurosci Lett* 248:109–112.
- Tu S, Okamoto S-I, Lipton SA, Xu H (2014) Oligomeric A β -induced synaptic dysfunction in Alzheimer's disease. *Mol Neurodegener* 9:1–12.
- Tzingounis A V., Wadiche JI (2007) Glutamate transporters: Confining runaway excitation by shaping synaptic transmission. *Nat Rev Neurosci* 8:935–947.
- Ueda Y, Doi T, Tsuru N, Tokumaru J, Mitsuyama Y (2002) Expression of glutamate transporters and ionotropic glutamate receptors in GLAST knockout mice. *Brain Res Mol Brain Res* 104:120–126.
- Vandenberg RJ, Ryan RM (2013) Mechanisms of glutamate transport. *Physiol Rev* 93:1621–1657.
- Varga E, Juhász G, Bozsó Z, Penke B, Fülöp L, Szegedi V (2015) Amyloid- β 1-42 disrupts synaptic plasticity by altering glutamate recycling at the synapse. *J Alzheimer's Dis* 45:449–456.
- Volianskis A, Bannister N, Collett VJ, Irvine MW, Monaghan DT, Fitzjohn SM, Jensen MS, Jane DE, Collingridge GL (2013) Different NMDA receptor subtypes mediate induction of long-term potentiation and two forms of short-term potentiation at CA1 synapses in rat hippocampus in vitro. *J Physiol* 591:955–972.
- Volianskis A, France G, Jensen MS, Bortolotto ZA, Jane DE, Collingridge GL (2015) Long-term potentiation and the role of N-methyl-d-aspartate receptors. *Brain Res* 1621:5–16.
- Wang Y, Briz V, Chishti A, Bi X, Baudry M (2013) Distinct Roles for γ -Calpain and m-Calpain in Synaptic NMDAR-Mediated Neuroprotection and Extrasynaptic NMDAR-Mediated

Neurodegeneration. *J Neurosci* 33:18880–18892 Available at:

<http://www.jneurosci.org/cgi/doi/10.1523/JNEUROSCI.3293-13.2013>.

Wang Y, Mattson MP (2014) L-type Ca²⁺ currents at CA1 synapses , but not CA3 or dentate granule neuron synapses , are increased in 3xTgAD mice in an age-dependent manner. *Neurobiol Aging* 35:88–95.

Wang Y, Zhu G, Briz V, Hsu Y-T, Bi X, Baudry M (2014) A molecular brake controls the magnitude of long-term potentiation. *Nat Commun* 5:3051.

Watabe AM, Carlisle HJ, O'Dell TJ (2002) Postsynaptic induction and presynaptic expression of group 1 mGluR-dependent LTD in the hippocampal CA1 region. *J Neurophysiol* 87:1395–1403.

Watase K, Hashimoto K, Kano M, Yamada K, Watanabe M, Inoue Y, Okuyama S, Sakagawa T, Ogawa SI, Kawashima N, Hori S, Takimoto M, Wada K, Tanaka K (1998) Motor discoordination and increased susceptibility to cerebellar injury in GLAST mutant mice. *Eur J Neurosci* 10:976–988.

Welsby PJ, Rowan MJ, Anwyl R (2007) Beta-amyloid blocks high frequency stimulation induced LTP but not nicotine enhanced LTP. *Neuropharmacology* 53:188–195.

Xing J, Ginty DD, Greenberg ME (1996) Coupling of the RAS-MAPK pathway to gene activation by RSK2, a growth factor-regulated CREB kinase. *Science* 273:959–963.

Xu J, Kurup P, Zhang Y, Goebel-Goody SM, Wu PH, Hawasli AH, Baum ML, Bibb JA, Lombroso PJ (2009) Extrasynaptic NMDA Receptors Couple Preferentially to Excitotoxicity via Calpain-Mediated Cleavage of STEP. *J Neurosci* 29:9330–9343

Available at: <http://www.jneurosci.org/cgi/doi/10.1523/JNEUROSCI.2212-09.2009>.

Yi J-H, Hazell AS (2006) Excitotoxic mechanisms and the role of astrocytic glutamate transporters in traumatic brain injury. *Neurochem Int* 48:394–403.

Zhu G, Liu Y, Wang Y, Bi X, Baudry M (2015) Different patterns of electrical activity lead to long-term potentiation by activating different intracellular pathways. *J Neurosci* 35:621–633.